

Review

Design and Synthesis of Photoactive Iron *N*-Heterocyclic Carbene Complexes

Simon Kaufhold  and Kenneth Wärnmark * 

Centre for Analysis and Synthesis, Lund University, Box 124, 22100 Lund, Sweden; simon.kaufhold@chem.lu.se

* Correspondence: kenneth.warnmark@chem.lu.se; Tel.: +46-46-22-8217

Received: 26 December 2019; Accepted: 13 January 2020; Published: 17 January 2020



Abstract: The use of iron in photoactive metal complexes has been investigated for decades. In this respect, the charge transfer (CT) states are of particular interest, since they are usually responsible for the photofunctionality of such compounds. However, only recently breakthroughs have been made in extending CT excited state lifetimes that are notoriously short-lived in classical polypyridine iron coordination compounds. This success is in large parts owed to the use of strongly σ -donating *N*-heterocyclic carbene (NHC) ligands that help manipulating the photophysical and photochemical properties of iron complexes. In this review we aim to map out the basic design principles for the generation of photofunctional iron NHC complexes, summarize the progress made so far and recapitulate on the synthetic methods used. Further, we want to highlight the challenges still existing and give inspiration for future generations of photoactive iron complexes.

Keywords: iron; *N*-heterocyclic carbenes; NHCs; coordination chemistry; photophysics; photochemistry

1. Introduction

Photoactive coordination compounds have been the subject of research for several decades, and led to their application in light emitting devices, optical sensors, photoactive drugs and as photosensitizers (PS) in light-driven organic transformations or artificial photosynthesis reactions as well as in photovoltaic devices. Especially the field of photoredox catalysis and artificial photosynthesis have seen rapid developments over the past decade [1–5]. This success is related to the beneficial photoproperties, i.e., long-lived and high energy metal-to-ligand charge transfer (MLCT) states, of the often used complexes of Ru(II), Ir(III), Os(II) or Re(I) featuring $4d^6$ or $5d^6$ electron configuration and ligands based on polypyridines and their derivatives [6,7]. However, the scarcity and related cost of these elements are detrimental to their application on a large scale. In recent years the interest in replacing rare metals by more earth abundant alternatives has been growing significantly and successful strategies have been reported for a range of 3d transition metals and relatively abundant heavier metals such as Zr, Mo, Ce, W or U [8–10]. Iron takes a special role in this context, as it is the fourth most common element in the Earth's crust and it is the 3d congener of ruthenium and should thus have similar chemical properties [11]. However, the electronic structure of Fe(II) polypyridine complexes is inherently different from their Ru(II) analogues making them far less useful in photochemical applications. In the following chapters, we aim to explain in simple terms these fundamental differences and resulting difficulties to generate viable photoactive iron complexes, present strategies to overcome these issues, summarize the progress made so far and give inspiration for new generations of photofunctional iron complexes. For a more detailed description of the photophysical aspects, the reader is referred to the complementary review by Persson and Sundström et al. [12] in this issue of *Catalysts* and a recent concept article by Wenger [13].

2. Fundamental Considerations

An ideal photosensitizer should efficiently absorb light and transform all the captured energy into a readily utilizable form while maintaining its molecular integrity. Clearly, the broader the absorption spectrum and the higher the likelihood for a photon of a certain wavelength to be absorbed, the more of the energy of the light can in principle be utilized for a light-driven process. However, the excited state generated by the absorption needs to be of a kind that makes this utilization feasible, ideally by spatially separating the excited electron from the created hole for an amount of time that allows for a reaction, or further charge separation, to take place. However, all of this is not of much use, if the excited state energy does not match the requirements for a certain task, e.g., the electron injection into the conduction band of a semiconductor or oxidation of a substrate molecule. More precisely, the following criteria should be fulfilled by the photosensitizer molecule to the best possible extent:

- Absorption of light over a broad range of the spectrum of the light source (visible and near-infrared in the context of solar energy conversion);
- Strong absorption of light, i.e., high molar attenuation coefficients;
- Formation of long-lived (usually n– μ s timescale) excited states of charge transfer (CT) character;
- Suitable ground and excited state redoxpotentials;
- Long-term chemical and photo-stability.

These criteria are quite well fulfilled for $[\text{Ru}(\text{bpy})_3]^{2+}$ (bpy = 2,2'-bipyridine) and its derivatives. They exhibit strong absorption over a rather broad range of the solar spectrum and form photoluminescent CT excited states of a typically several 100 ns lifetime. Further, these states are reducing/oxidizing enough to drive water splitting reactions under the right conditions or inject electrons into a semiconductor surface and be regenerated by common redox mediators. However, depending on conditions, photostability can be an issue [6]. A simplified schematic presentation of the excited state energy landscape of a typical Ru polypyridine complex can be seen in Figure 1a and is explained in more detail below.

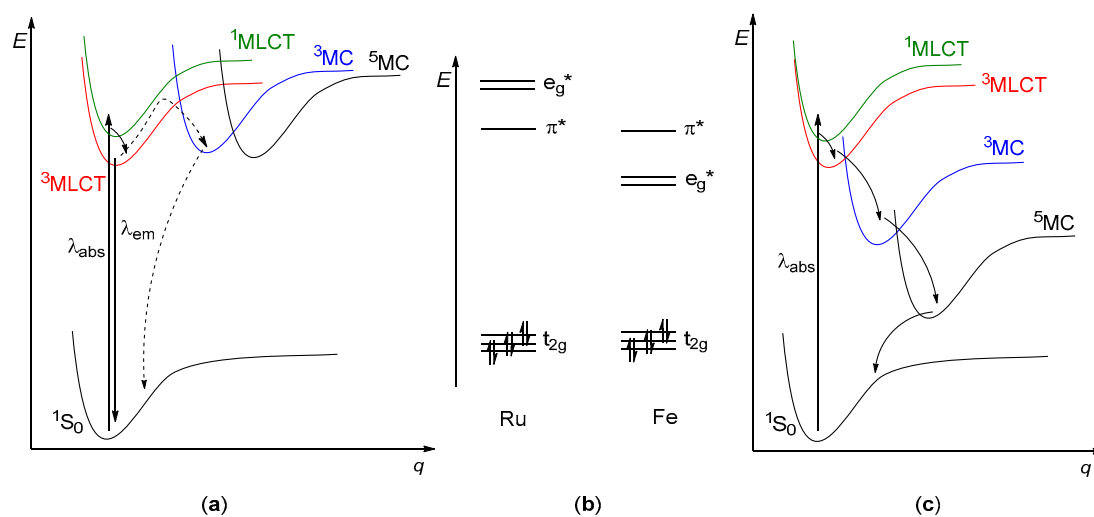


Figure 1. (a) Schematic excited state energy landscape of Ru polypyridine complexes (b) corresponding simplified MO scheme for Ru and Fe complexes (c) schematic excited state energy landscape for Fe polypyridine complexes.

In an octahedral ligand field, the d orbitals split into the t_{2g} and e_g levels. The symmetry of the complexes mentioned here is lower than octahedral due to the use of bi- or tridentate ligands. Even though the designation as t_{2g} and e_g is thus not fully accurate, for better readability we will refer to molecular orbitals derived from d_{xy} , d_{xz} and d_{yz} as t_{2g} and those derived from $d_{x^2-y^2}$ and d_z^2 as e_g (or e_g^* as they are usually anti-bonding). The metal–ligand interactions are stronger in 4d and 5d metal complexes compared to the 3d analogs, resulting in a stronger ligand field splitting for the former case, and hence formation of low-spin complexes [14]. Importantly, in $[\text{Ru}(\text{bpy})_3]^{2+}$ the e_g^* orbitals are well-separated from the t_{2g} orbitals and higher in energy than the π^* orbitals of the bipyridine ligands, therefore the lowest unoccupied molecular orbital (LUMO) is based on the ligand (Figure 1b). Ru(II) in $[\text{Ru}(\text{bpy})_3]^{2+}$ has six d-electrons which results in a t_{2g}^6 electron configuration, so the highest occupied molecular orbital (HOMO) has metal character. The minimum energy transition upon absorption of a photon (= HOMO to LUMO excitation) for an electron is thus a MLCT. During the excitation the spin multiplicity remains the same as in the ground state (both are singlet: $^1S_0 \rightarrow ^1\text{MLCT}$). However, intersystem crossing (ISC) on an ultrafast timescale results in a spin flip and leads to the population of a more stable triplet MLCT ($^3\text{MLCT}$) state. As this is the excited state of lowest energy in $[\text{Ru}(\text{bpy})_3]^{2+}$, any molecule will end up in this state eventually according to Kasha's rule, even if excited at higher energies. This also means that the energy conserved in the $^3\text{MLCT}$ state is what is available to drive a photoinduced process and that a longer $^3\text{MLCT}$ lifetime will give a higher chance for this process to happen. Interfering metal centered (MC) triplet or quintet states ($^3\text{MC}/^5\text{MC}$) are usually responsible for fast, radiationless depopulation of excited states. In $[\text{Ru}(\text{bpy})_3]^{2+}$ the MC states are similar or higher in energy than the MLCT states and thus an activation barrier has to be overcome to populate these MC states (c.f., dashed arrows in Figure 1a). This in turn leads to long-lived (hundreds of ns), emissive $^3\text{MLCT}$ states.

The isoelectronic 3d iron polypyridine complex $[\text{Fe}(\text{bpy})_3]^{2+}$ has a significantly smaller ligand field splitting due to diminished orbital overlap [14]. Thus, the e_g^* orbitals are lower in energy than the π^* ligand orbitals resulting in low-lying MC states (Figure 1b). Even though the MLCT states are initially populated (the d-d transitions between t_{2g} and e_g^* orbitals are Laporte-forbidden), the barrierless transition to the lower lying MC states leads to fast (sub-ps timescale), radiationless deactivation of the excited state (visualized by full arrows in Figure 1c) [15]. Although this phenomenon of populating high-spin states in this way (light-induced excited-state spin trapping = LIESST) is explored for spintronics and data-storage applications, it is detrimental for energy conversion purposes [16–18].

In a simplified picture to counteract the problem of fast deactivation, the position of the MC states relative to the MLCT states must be reversed. This can be done by either destabilizing/pushing up the MC states to higher energy or by stabilizing/lowering down the MLCT states. However, as the $^3\text{MLCT}$ is also the photoactive state, it should not be too low in energy as this would limit the driving-force for the photoprocess.

Increasing the energy of the e_g^* orbitals and thus the related MC states can be achieved by introducing a stronger ligand field, e.g., by using strongly σ -donating ligands. The extra electron density provided to the metal center destabilizes (mostly) the orbitals along the ligand coordinates, namely $d_{x^2-y^2}$ and d_z^2 , corresponding to the e_g^* orbitals. Further, arrangement of the ligands around the metal center as close as possible to perfect octahedral geometry will enhance ligand field splitting as well, as the orbital interaction between ligand and metal is maximized (Figure 2).

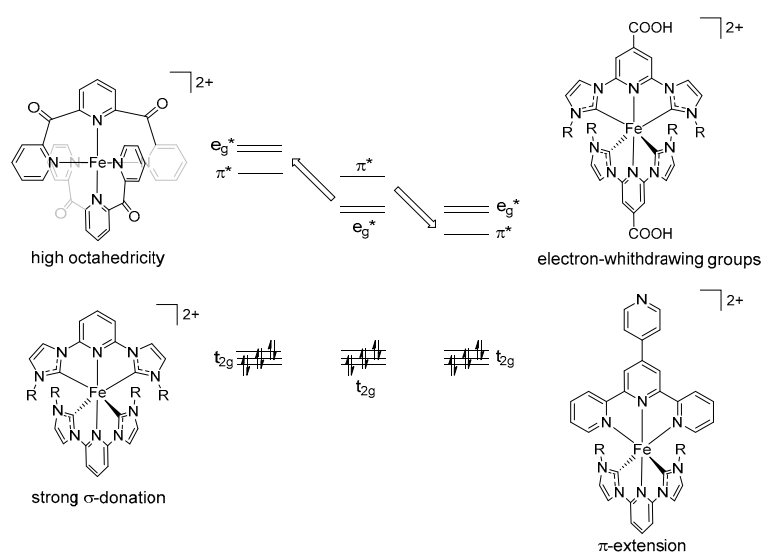


Figure 2. Ligand-design strategies to destabilize metal centered (MC) or stabilize metal-to-ligand charge transfer (MLCT) states in metal complexes [19–24].

To stabilize the MLCT state, the π^* orbital of the ligands must be lowered in energy. One way to achieve this is by increasing the size of the ligand π system as this will bring the π and π^* levels closer together as rationalized by molecular orbital (MO) theory [25]. The introduction of electron-withdrawing groups (EWGs) on the ligands has a similar effect; however, in this case the π^* as well as π levels will be pulled down in energy. This can also be rationalized by the removal of electron density from the π system which makes it easier to transfer an extra electron onto it.

The mentioned (and further [26]) concepts have all been used and the photophysical properties of the generated iron complexes have been investigated: the use of strongly σ -donating ligands has also been demonstrated by replacing two bpy ligands in $[\text{Fe}(\text{bpy})_3]^{2+}$ by four strongly σ -donating CN^- ligands, generating the heteroleptic complex $[\text{Fe}(\text{bpy})(\text{CN})_4]^{2-}$ showing a MLCT excited state lifetime in the order of picoseconds [27]. The homoleptic complex $[\text{Fe}(\text{dcpp})_2]^{2+}$ (dcpp = 2,6-bis(2-carboxypyridyl)pyridine) [22], and the heteroleptic push-pull complex $[\text{Fe}(\text{dcpp})(\text{ddpd})]^{2+}$ (ddpd = *N,N'*-dimethyl-*N,N'*-dipyridine-2-yl-pyridine-2,6-diamine) were prepared and showed increased octahedricity, leading to a stronger ligand field compared to conventional 2,2':6',2''-terpyridine (tpy) [23,28]. Further, dcpp features EWG and ddpd electron-donating groups (EDG) to influence π -accepting and σ -donating properties of the ligands, respectively. Unfortunately, the lifetime of the MLCT state was not increased significantly in these complexes. Thus, the use of strongly σ -donating *N*-heterocyclic carbene (NHC) ligands has so far been the most successful strategy to increase the excited state lifetime of CT states, c.f., [13,29] (and references therein) and below. Excited state dynamics of 3d transition metal complexes tend to be complicated and often happen on ultrafast timescales (several 10s of fs to ps). Clearly, the whole excited state landscape influences decay paths and the lifetime of the intermediate states, however, for simplicity we generally use the CT state lifetimes as a benchmark in this review as this is also the state deemed most relevant for photophysical applications like sensitization in dye-sensitized solar cells (DSSCs) or photocatalytic conversions.

As described above, the excited state properties can be steered by ligand design to a great extent. However, incorporating all beneficial properties in one ligand is not as trivial as it might seem, as there are collateral influences that need to be considered and could be detrimental to the overall intent. For example, while NHCs are stronger σ donors than (poly)pyridines, their π system is smaller and thus their LUMO is significantly higher in energy. Therefore, the beneficial influence on the energy of the MC states is to some extent counteracted by the adverse effect on the MLCT states, as both states are pushed up in energy. Additionally, the energy of the t_{2g} orbitals is influenced. As the typical imidazole-derived NHC is a rather poor π acceptor the high electron density on the metal center

also leads to an increase of the energy level of the t_{2g} orbitals, which results in a shift of the Fe(III/II) oxidation potential to more negative/cathodic values. Consequently, both HOMO and LUMO levels are influenced, which results in a change of the HOMO–LUMO gap and its absolute position. In that regard, the original intent of prolonging the excited state lifetime of the PS leads to a collateral change of its absorption and redox properties which further on is bound to influence the potential substrate scope in a photocatalytic reaction or influence the choice of semiconductors or redox mediators in a DSSC incorporating this PS. So far design strategies have mostly focused on the extension of excited state lifetimes, however, in the future a more holistic approach will be necessary to control all wanted properties. Additionally, the symmetry (and thus potentially isomerism) of a metal complex also has an influence on the (excited) state landscape as briefly discussed in the last paragraphs of Section 4. In Appendix A (Table A1) a table is given summarizing absorption characteristics, CT state lifetimes and the redox potentials of the Fe(III/II) couple for the discussed complexes.

3. FeNHC Complexes with Meridional Coordinating Tridentate Ligands

3.1. Homoleptic FeNHC Complexes with Meridional Coordinating Tridentate Ligands

The first examples of iron complexes making use of NHC ligands to enhance photophysical properties were presented in 2013 [21]. The ligands are congeners of the archetype tpy structure and feature a central pyridine ring with two imidazole rings attached. Substitution of the exo-positioned nitrogen atom of the imidazole units by alkyl or aryl groups leads to an imidazolium salt as the carbene precursor. After deprotonation and formation of the imidazolylidene this results in a CNC coordination (in contrast to the NNN coordination of tpy). In this first study the imidazolylidene units were N-substituted by either Me or *t*Bu groups, leading to $[\text{Fe}(\text{pbmi})_2]^{2+}$ and $[\text{Fe}(\text{pbbi})_2]^{2+}$ (pbmi = (pyridine-2,6-diyl)bis(1-methyl-imidazol-2-ylidene), pbbi = (pyridine-2,6-diyl)bis(1-*tert*-butyl)-imidazol-2-ylidene)) which were compared to $[\text{Fe}(\text{tpy})_2]^{2+}$ (Figure 3).

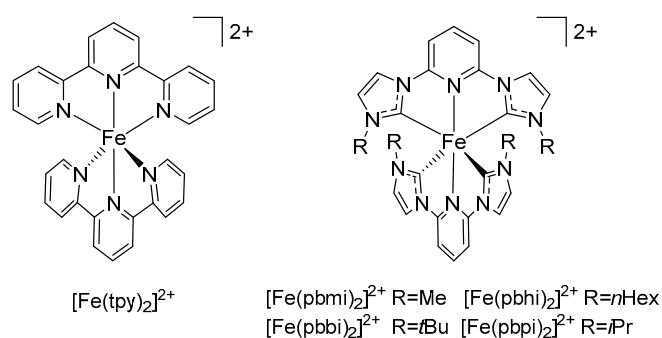


Figure 3. Parental $[\text{Fe}(\text{tpy})_2]^{2+}$ and homoleptic FeNHC complexes featuring CNC ligands with different N-substituents [20,21,24].

From a design perspective the introduction of the NHC moieties should significantly increase the ligand field splitting while the pyridine moiety featuring relatively low π^* levels should accommodate the excited electron. Transient absorption (TA) spectroscopy revealed that $[\text{Fe}(\text{tpy})_2]^{2+}$ undergoes ultrafast decay (145 fs) of the $^3\text{MLCT}$ state to a MC state after photoexcitation. In $[\text{Fe}(\text{pbbi})_2]^{2+}$ the lifetime of the MLCT state is roughly twice as long (300 fs) [21]. Due to the bulky *t*Bu groups in $[\text{Fe}(\text{pbbi})_2]^{2+}$ short Fe–C bonds and thus strong metal–ligand interactions are hindered which in turn explains the rather small ligand effect on the $^3\text{MLCT}$ lifetime in $[\text{Fe}(\text{pbbi})_2]^{2+}$. This is different in $[\text{Fe}(\text{pbmi})_2]^{2+}$ featuring sterically less demanding Me groups as N-substituents, which allows for a much stronger metal–ligand interaction leading to a significantly increased $^3\text{MLCT}$ lifetime of 9 ps [21]. For iron complexes with low ligand field splitting the following deactivation cascade is usually envisaged: excitation into $^1\text{MLCT} \rightarrow ^3\text{MLCT} \rightarrow ^3\text{MC} \rightarrow ^5\text{MC} \rightarrow \text{GS}$ (ground state, c.f., Figure 4a).

However, the decay of the $^1\text{MLCT}$ and ^3MC state is often so fast (<100 fs) that these components are not resolved experimentally while the lifetime of the ^5MC state can be in the order of a few ns. $[\text{Fe}(\text{pbbi})_2]^{2+}$ is a somewhat special case as the ligands contain strongly σ -donating NHC moieties, however, the steric demand of the *t*Bu groups diminishes their influence. In a later study time-resolved wide-angle X-ray scattering (TRWAXS) and density functional theory (DFT) calculations were used to gain more insight into the excited state (structural) dynamics [30]. It was established, that the longest time component found earlier (230 ps) [21], is indeed connected to a ^5MC state (here 260 ps) that is positioned 0.75 eV above the GS. Population of this state is accompanied by strong structural changes of the complex, namely elongation and twisting of all metal–ligand bonds [30]. This is a difference distinguishing $[\text{Fe}(\text{pbbi})_2]^{2+}$ from most other FeNHC complexes reported later where usually ^3MC states are crucial for the excited state deactivation (see also the following paragraph).

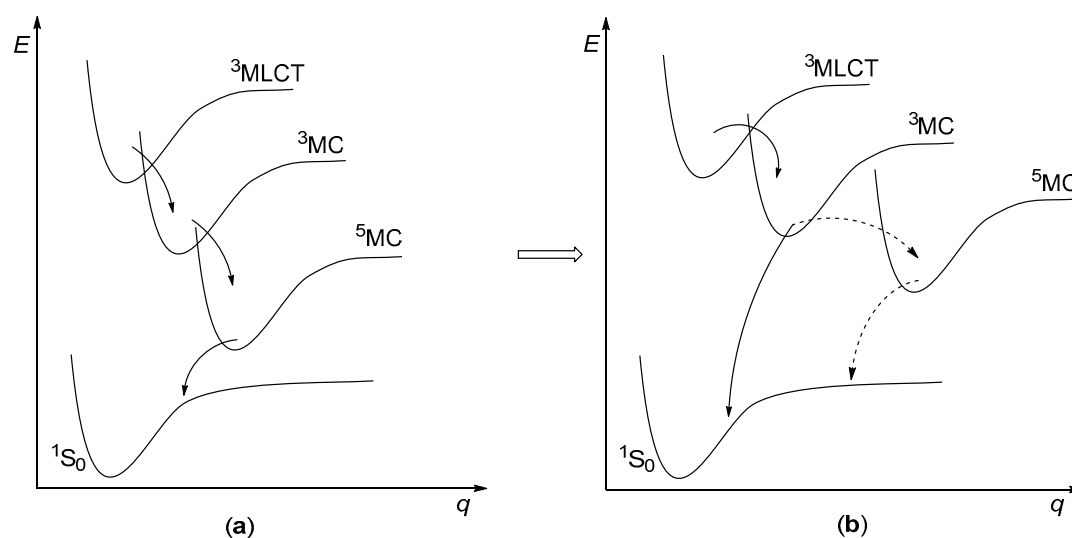


Figure 4. Influence on the MC state energy and position by introduction of strongly σ -donating ligands. Both MC states are pushed up in energy going from (a,b), but the ^5MC state is moved further out on the reaction coordinate q becoming less accessible in the deactivation process.

The excited state landscape of $[\text{Fe}(\text{pbmi})_2]^{2+}$ was investigated in detail in a computational study using density functional theory (DFT) and time-dependent (TD-)DFT methods [31]. Strong interaction (σ -donation and π -backdonation) between ligand and metal center were verified as well as the assignment of the 9 ps lifetime to a $^3\text{MLCT}$ state by calculating the excited state potential energy surfaces (PESs) of the different states. It was also found that the MC states were indeed pushed to higher energies by the NHC ligands compared to $[\text{Fe}(\text{tpy})_2]^{2+}$. Additionally, the ^5MC state which is usually involved in the deactivation cascade of iron polypyridine complexes as outlined above, becomes inaccessible in $[\text{Fe}(\text{pbmi})_2]^{2+}$ as it is pushed “further out” on the reaction coordinate which describes the average bond length between the metal center and the ligand(s) (Figure 4b). The displacement can be explained by the strong structural rearrangements that the complex would undergo if two antibonding e_g^* orbitals were populated in the ^5MC state. It should also be noted that calculations of the spin-density distribution in the MC states showed that spin-density is not only located on the metal center but also on the coordinating carbene C atoms, which is explained by the strong metal–ligand interaction (= high covalency). Thus, the localization of a state as purely metal or ligand centered is sometimes not as clear-cut as in traditional coordination compounds, which should be kept in mind when the character of an excited state is discussed.

The *n*-hexyl *N*-substituted compound $[\text{Fe}(\text{pbhi})_2]^{2+}$ (pbhi = (pyridine-2,6-diyl)bis(1-hexyl-imidazol-2-ylidene)) (Figure 3) was presented in 2014 [20]. The long alkyl chains are less bulky than the *t*Bu-group in $[\text{Fe}(\text{pbbi})_2]^{2+}$. So, as expected the ground state properties are very similar to those of $[\text{Fe}(\text{pbmi})_2]^{2+}$: the oxidation of the Fe(II) metal center to Fe(III) appears at a slightly more positive

potential of 0.41 V (in MeCN vs. Fc^+/Fc) compared to 0.31 V for $[\text{Fe}(\text{pbmi})_2]^{2+}$ in cyclic voltammetry (CV) measurements. Absorption bands of CT character appear at 393 and 460 nm (vs. 390 and 457 nm for $[\text{Fe}(\text{pbmi})_2]^{2+}$) with molar attenuation coefficients between 9000 and 15000 $\text{M}^{-1} \text{cm}^{-1}$. However, no excited state lifetimes were reported for $[\text{Fe}(\text{pbhi})_2]^{2+}$ [20].

$[\text{Fe}(\text{pbpi})_2]^{2+}$ pbpi = (pyridine-2,6-diyl)bis(1-isopropyl-imidazol-2-ylidene)) (Figure 3) is another example of a homoleptic FeNHC complex and was recently presented in the first study using FeNHCs as photosensitizers for hydrogen gas formation [24]. The isopropyl N-substituents do not seem to introduce strong steric hindrance, as the average Fe-C(NHC) bond lengths (1.952 Å) are much closer to those of $[\text{Fe}(\text{pbmi})_2]^{2+}$ (1.967 Å) than of $[\text{Fe}(\text{pbbi})_2]^{2+}$ (2.096 Å) [21,24]. However, the Fe(III/II) redox couple appears at 0.43 V (vs. Fc^+/Fc) and is thus almost identical to that of $[\text{Fe}(\text{pbhi})_2]^{2+}$ [20,24]. It could be hypothesized that the intermediate steric bulk of *n*-hexyl and isopropyl groups does not influence the bond length and thus σ -donor strengths significantly but leads to some shielding of the metal center and thereby shifting the potential to more anodic/positive potentials compared to $[\text{Fe}(\text{pbmi})_2]^{2+}$. The position of the MLCT absorption bands (392 and 458 nm) and attenuation coefficients (9000–15000 $\text{M}^{-1} \text{cm}^{-1}$) of $[\text{Fe}(\text{pbpi})_2]^{2+}$ are close to those reported for similar complexes mentioned earlier. TD-DFT calculations and various different X-ray spectroscopic methods support the MLCT character of these bands [24,32]. The lifetime of the $^3\text{MLCT}$ state was found to be 8.1 ps which is close to that of similar complexes like $[\text{Fe}(\text{pbmi})_2]^{2+}$ (9 ps) [21,32].

An approach leading to an extended ligand π system is to decorate bpy with a methyl-imidazolylidene unit leading to the bpymi ligand (bpymi = (([2,2'-bipyridin]-6-yl)-3-methyl-imidazol-2-ylidene)) and the iron complex $[\text{Fe}(\text{bpymi})_2]^{2+}$ (Figure 5). This complex was presented in a study comparing FeNHC complexes with a varying number of NHC groups in their ligand environment [32]. The steady-state absorption spectrum of this compound shows MLCT bands at 419, 508 and 557 nm. CV measurements reveal two reversible signals in the negative potential range (−1.74 and 2.02 V vs. Fc^+/Fc) correlated to the reduction of the two bpy units in the complex. In comparison, the reduction of pbRi-type ligands (pbRi = (pyridine-2,6-diyl)bis(1-alkyl/aryl-imidazol-2-ylidene)) in the corresponding complexes are usually irreversible and appear at more negative potentials between −2.3 to −2.4 V vs. Fc^+/Fc [21,32,33]. Interestingly, the Fe(III/II) oxidation appears at 0.44 V vs. Fc^+/Fc and is thus quite similar to that of $[\text{Fe}(\text{pbmi})_2]^{2+}$ (0.31 V vs. Fc^+/Fc) even though $[\text{Fe}(\text{bpymi})_2]^{2+}$ features only two instead of four NHC moieties [21,32]. Consequently, the HOMO–LUMO gap is relatively small in $[\text{Fe}(\text{bpymi})_2]^{2+}$ leading to the rather low-energy MLCT transitions mentioned above. An excited state lifetime of 96 ps was observed but assigned to a state of MC- instead of MLCT character. Assignment and energy of the states were also investigated by a range of X-ray spectroscopy methods and TD-DFT calculations, supporting these conclusions [32]. It can be summarized that the π -extension approach is successful in terms of increasing the absorption window; however, the presence of only two NHC moieties in the coordination sphere does not seem to destabilize the MC states in a sufficient manner to generate long-lived photoactive MLCT excited states.

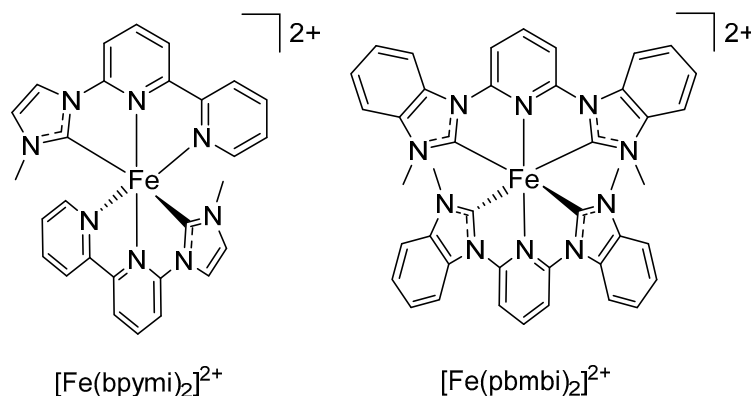


Figure 5. Different approaches to modify the ligand π system of FeNHC complexes [32,33].

A modification to the π system of CNC-type ligands without changing the number of NHC moieties was presented in 2016 by exchanging imidazolylidene for benzimidazolylidene moieties, leading to $[\text{Fe}(\text{pbmbi})_2]^{2+}$ (pbmbi = (pyridine-2,6-diyl)bis(1-methyl-benzimidazol-2-ylidene), Figure 5) [33]. Compared to parental $[\text{Fe}(\text{pbmi})_2]^{2+}$ (393 and 460 nm), a small blueshift of the MLCT absorption bands is observed for $[\text{Fe}(\text{pbmbi})_2]^{2+}$ (360 and 440 nm). In CV measurements, the Fe(III/II) couple of $[\text{Fe}(\text{pbmbi})_2]^{2+}$ appears at 1.04 V (vs. saturated calomel electrode = SCE, 0.65 V vs. Fc^+/Fc) and is thus shifted to more positive potentials by more than 0.2 V compared to $[\text{Fe}(\text{pbmi})_2]^{2+}$ (0.8 V vs. SCE, 0.41 vs. Fc^+/Fc). The first reduction waves appear at -1.8 V and -1.95 V vs. SCE (-2.19 and -2.34 V vs. Fc^+/Fc), respectively, resulting in a smaller change of 0.15 V compared to $[\text{Fe}(\text{pbmi})_2]^{2+}$ [33]. Thus, for $[\text{Fe}(\text{pbmbi})_2]^{2+}$ the following picture can be drawn (visualized in Figure 6): even though the ligand-based LUMO level is lowered by extending the π system as reflected in the less negative reduction potential (easier to reduce), the HOMO–LUMO gap becomes larger (hypsochromic shift, sometimes also called blueshift, in MLCT absorption bands), as the stabilization of the t_{2g} orbitals (HOMO) by the stronger π -accepting capability of the benzimidazolylidene units is more significant.

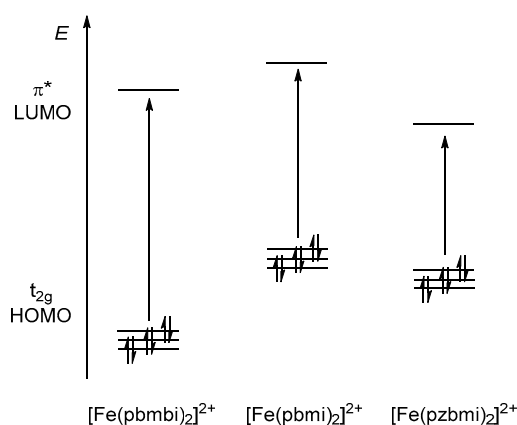


Figure 6. Visualization of a larger highest occupied molecular orbital (HOMO)–lowest unoccupied molecular orbital (LUMO) gap responsible for the hypsochromic shift of MLCT absorption bands for $[\text{Fe}(\text{pbmbi})_2]^{2+}$ compared to $[\text{Fe}(\text{pbmi})_2]^{2+}$ and smaller gap due to lower π^* orbital energy in $[\text{Fe}(\text{pzbmi})_2]^{2+}$ and related complexes.

The lifetimes of the $^3\text{MLCT}$ states were in this study found to be 10 ps for $[\text{Fe}(\text{pbmi})_2]^{2+}$ and 16 ps for $[\text{Fe}(\text{pbmbi})_2]^{2+}$ as established by TA spectroscopy [33]. This is an indication that the MLCT states have been stabilized compared to the MC states by lowering the LUMO energy. Some support for this comes from a computational study using charge displacement analysis to rationalize σ - and π -donating/accepting capabilities of NHC ligands that found that the σ -donation strength is the same for a benzimidazolylidene-based NHC ligand compared to an imidazolylidene-based, while the π -accepting capability is slightly stronger for the former [34].

Altering the central six-membered ring of CNC ligands is another approach to modifying the π properties. A series of complexes following this concept by replacing the pyridine ring with pyrazine or pyrimidine was recently published and led to the structures shown in Figure 7 [35]. Steady state absorption spectra show a bathochromic shift (sometimes also called redshift) of the low-energy MLCT band of 30–40 nm for all these complexes compared to $[\text{Fe}(\text{pbmi})_2]^{2+}$. This indicates that the additional heteroatom in the six-membered ring lowers the energy of the π^* orbitals more significantly than the energy of the t_{2g} orbitals and thus decreases the HOMO–LUMO gap (c.f., Figure 6). This is also reflected in the electrochemical bandgap – the difference between the first oxidation and reduction wave in CV, which is often used to estimate the HOMO–LUMO gap by electrochemical means. This gap is smaller for the newly reported complexes in comparison to the parental complex $[\text{Fe}(\text{pbmi})_2]^{2+}$ as the reduction is more significantly anodically shifted (= to more positive potentials) than the oxidation [35].

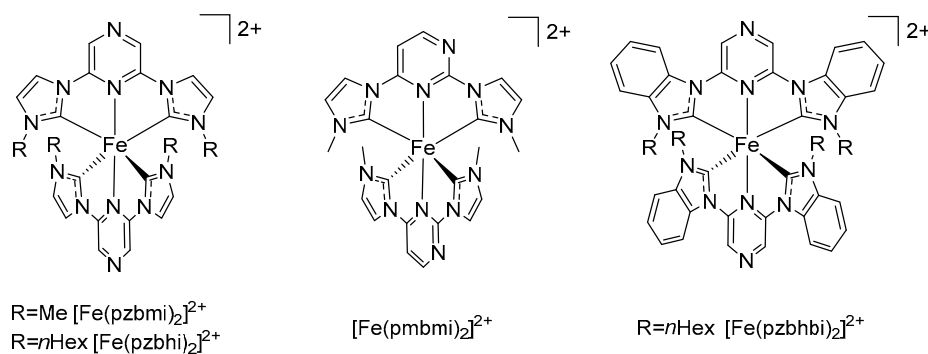


Figure 7. Complexes with variation of the central six-membered ring influencing the π system [35].

Similar to the effects described above for $[\text{Fe}(\text{pmbmi})_2]^{2+}$, the MLCT absorption bands of the benzimidazolylidene containing complex $[\text{Fe}(\text{pzbhbi})_2]^{2+}$ (pzbhbi = (pyrazine-2,6-diyl)bis(1-hexyl-benzimidazol-2-ylidene)) (Figure 7) are hypsochromically shifted compared to $[\text{Fe}(\text{pzbhi})_2]^{2+}$ (pzbhi = (pyrazine-2,6-diyl)bis(1-hexyl-imidazol-2-ylidene)) (Figure 7). Again, in this case, the π -accepting properties of the ligand lead to a more significant stabilization of the t_{2g} orbitals than of the π^* orbitals. Some distinctive features can be seen in the steady state absorption spectrum of $[\text{Fe}(\text{pmbmi})_2]^{2+}$ (pmbmi = (pyrimidine-2,4-diyl)bis(1-methyl-imidazol-2-ylidene)) (Figure 7). Both MLCT bands (reflecting transitions from Fe to NHC and pyrimidine moieties, respectively) are not only shifted to longer wavelengths but also broadened compared to parental $[\text{Fe}(\text{pbmi})_2]^{2+}$. This was explained by the reduced symmetry of the complex induced by the 2,4-substitution pattern of the pyrimidine ring. TA spectroscopy was used to investigate the excited state dynamics of the presented compounds. For $[\text{Fe}(\text{pzbhi})_2]^{2+}$ and $[\text{Fe}(\text{pzbhbi})_2]^{2+}$ the longest components of the excited state decay were established to be 23 and 33 ps, respectively. The involved states have triplet multiplicity, however, undergoing a MLCT \rightarrow MC conversion when progressing along the reaction coordinate. Introduction of the pyrazine and *n*-hexyl moieties quite significantly increases the longest lifetime compared to parental $[\text{Fe}(\text{pbmi})_2]^{2+}$ (around 9 ps) and $[\text{Fe}(\text{pmbmi})_2]^{2+}$ (16 ps) [21,33,35]. As the long time component of $[\text{Fe}(\text{pzbmi})_2]^{2+}$ (pzbmi = (pyrazine-2,6-diyl)bis(1-methyl-imidazol-2-ylidene)) (Figure 7) was found to be in the range of 21 to 25 ps, most of the influence seems to stem from the changes induced by alteration of the six-membered ring [35]. The lifetimes are given as a range here because the dynamics are varying slightly for different probe wavelengths. This behavior was ascribed to structural rearrangement of the complex in the excited state. Similar observations were made for the pyrimidine congener $[\text{Fe}(\text{pmbmi})_2]^{2+}$: while for most other compounds mentioned in this review the faster time components are not stated (and sometimes are even not resolved in the experiments), here it is worthwhile to take a closer look: two components in the ps-range (2–6 and 11–12 ps) were found for $[\text{Fe}(\text{pmbmi})_2]^{2+}$ of which the first is possibly associated to internal conversion (IC) to the ground state which is taking place in parallel to the “normal” intersystem crossing (ISC) from the $^3\text{MLCT}$ state. This parallel decay suggested here is rather uncommon; as mentioned in Section 2 a sequential decay is usually assumed/found for FeNHC complexes. In the present case it was hypothesized that upon electron transfer on the six-membered ring in the excited state, the aromaticity of the π system is broken leading to an out of plane (puckering) deformation of the ring resulting in a change of the Fe–N bond length. This has an influence on the excited state landscape and makes crossings from the triplet excited state to the singlet ground state more accessible. In the case of $[\text{Fe}(\text{pmbmi})_2]^{2+}$, featuring the asymmetric pyrimidine ring, more electron density is located on the nitrogen atoms close to the metal center, resulting in a stronger puckering motion. This explains why the effect on the excited state lifetimes is most pronounced for $[\text{Fe}(\text{pmbmi})_2]^{2+}$. In the complexes containing *n*-hexyl instead of methyl substituents, such puckering motion could be sterically hindered to some extent, explaining the sequential decay of the excited state and longer lifetimes found for complexes with *n*-hexyl

substituents. Further, the benzimidazolylidene moieties in $[\text{Fe}(\text{pzbhbi})_2]^{2+}$ can accept additional electron density, minimizing the detrimental effects for this complex and explaining its superior lifetime [35] compared to the other complexes presented in this paragraph. A further example of parallel decay will be explained in some more detail below (see Section 4).

3.2. Heteroleptic FeNHC Complexes with Meridional Tridentate Ligands

Heteroleptic complexes offer the possibility to modulate the properties of the complex by choice of the different ligands and their separate modification. In this way push–pull factors can be introduced and a more precise tuning of the different properties of the complex can be achieved. The protonatable complex $[\text{Fe}(\text{pbhi})(\text{pytpy})]^{2+}$ (pytpy = 4'-(pyridin-4-yl)-2,2':6',2''-terpyridine) (Figure 8), bearing the tpy derivative (pytpy = 4'-(pyridin-4-yl)-2,2':6',2''-terpyridine) and one pbhi carbene ligand was presented in 2014 [20].

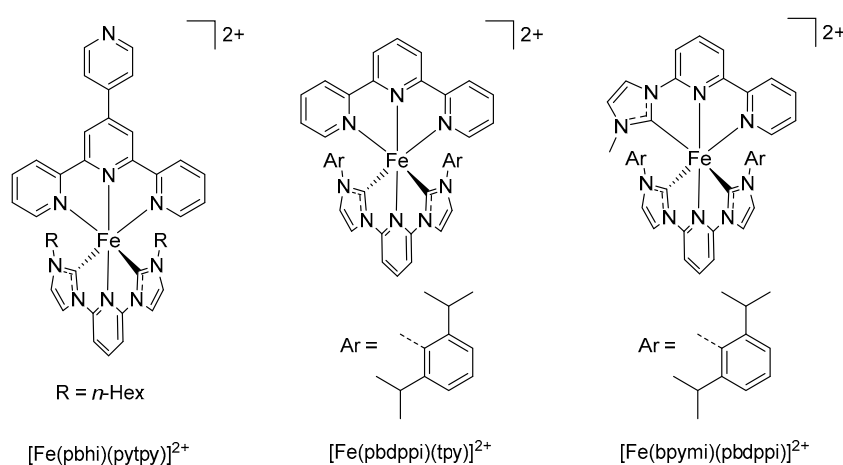


Figure 8. Heteroleptic FeNHC complexes featuring tpy and bpy derived ligands [20,24,32].

The pytpy ligand has rather low-lying π^* orbitals (compared to the pbhi carbene ligands) due to its extended π system. The introduction of this ligand leads to a significant bathochromic shift of the MLCT absorption bands from 393 and 460 nm to 522 and 560 nm without significantly decreasing the attenuation coefficients (9000 to 15000 $\text{M}^{-1} \text{cm}^{-1}$). The terminal pyridine unit of the pytpy ligand can be protonated which results in a further bathochromic shift of the absorption bands. Electrochemical data shows that the Fe(III/II) couple is more positive for $[\text{Fe}(\text{pbhi})(\text{pytpy})]^{2+}$ and its protonated version $[\text{Fe}(\text{pbhi})(\text{pytpyH})]^{3+}$ (0.54 and 0.56V vs. Fc^+/Fc) compared to the parent $[\text{Fe}(\text{pbhi})_2]^{2+}$ (0.41 V vs. Fc^+/Fc) bearing two carbene containing ligands. This reflects the stabilization of the HOMO levels by the more π -accepting and less σ -donating character of the pytpy ligand. The bathochromic shift of absorption bands in $[\text{Fe}(\text{pbhi})(\text{pytpy})]^{2+}$ and $[\text{Fe}(\text{pbhi})(\text{pytpyH})]^{3+}$ can then be explained by the more significantly lowered π^* orbital energy level (c.f., middle and right case in Figure 6). (TD-)DFT methods were used to calculate the natural transition orbitals (NTOs) of the investigated compounds. The occupied NTOs (oNTOs) of both, $[\text{Fe}(\text{pbhi})(\text{pytpy})]^{2+}$ and $[\text{Fe}(\text{pbhi})(\text{pytpyH})]^{3+}$, have mostly metal character with some delocalization on the ligands. These are the orbitals providing the electron that gets excited and thus represent the location of the hole in the excited state. In contrast, the virtual NTOs (vNTOs), that correspond to the orbitals accommodating the electron in the excited state, are mostly located on the pytpy ligand. This effect becomes more pronounced for $[\text{Fe}(\text{pbhi})(\text{pytpyH})]^{3+}$ due to the more electron-withdrawing character of the protonated ligand. Thus, the MLCT nature of the transition as well as the concept of introducing ligands with low-lying π^* orbitals to accommodate the excited state is consolidated. Unfortunately, no time-resolved spectroscopy was reported for these complexes to correlate the made observations to excited state lifetimes.

Another example of a heteroleptic FeNHC is $[\text{Fe}(\text{pbdppi})(\text{tpy})]^{2+}$ (pbdppi = (pyridine-2,6-diyl)bis(1-(2,6-diisopropylphenyl)-imidazol-2-ylidene)), depicted in Figure 8 [24]. This complex was also used for the light-driven reduction of protons. The choice of ligands was made with similar reasoning as above: the carbene ligand should destabilize MC states, while the tpy ligand should lead to increased light absorption and provide low-lying π^* orbitals. Indeed, the MLCT absorption bands of $[\text{Fe}(\text{pbdppi})(\text{tpy})]^{2+}$ (502 and 540 nm) are situated between those of $[\text{Fe}(\text{tpy})_2]^{2+}$ (552 nm) and $[\text{Fe}(\text{pbpi})_2]^{2+}$ (458 nm) that were investigated in the same study, while maintaining high attenuation coefficients of around $10000 \text{ M}^{-1} \text{ cm}^{-1}$ [24]. The MLCT character of these transitions was again supported by TD-DFT calculations. For $[\text{Fe}(\text{pbdppi})(\text{tpy})]^{2+}$ weak luminescence was found and time-correlated single photon counting (TCSPC) experiments revealed a 2.7 ns lifetime. However, the emission band appears at 343 nm and thus does not stem from the MLCT state but was tentatively assigned to a singlet ligand-centered (^1LC) transition. The performance of the mentioned compounds in hydrogen gas formation reactions was tested using $\text{H}_2\text{O}/\text{MeCN}$ (4:1) as solvent, NEt_3 as sacrificial electron donor and in situ formed platinum colloids as reduction catalyst. The investigations showed that $[\text{Fe}(\text{pbpi})_2]^{2+}$ slightly outperforms $[\text{Fe}(\text{pbdppi})(\text{tpy})]^{2+}$ in terms of efficiency in promoting hydrogen gas production. However, rather low turnover numbers ($\text{TON} = n(\text{H}_2)/n(\text{PS})$) of 4 ($[\text{Fe}(\text{pbpi})_2]^{2+}$) and 3 ($[\text{Fe}(\text{pbdppi})(\text{tpy})]^{2+}$) were found. Experiments with bandpass filters showed that the MLCT absorption is responsible for driving the hydrogen gas formation as the reaction was not influenced if light of $<520 \text{ nm}$ was cut out. Notably, the carbene containing PSs showed stability as their molecular integrity remained intact over the course of the reactions as proven by X-ray absorption spectroscopy (XAS) measurements [24]. In a later study, the MLCT lifetime of $[\text{Fe}(\text{pbdppi})(\text{tpy})]^{2+}$, featuring two carbene moieties in the ligand sphere, was estimated to be $<100 \text{ fs}$. This is much shorter than the 8 ps found for $[\text{Fe}(\text{pbpi})_2]^{2+}$ containing four carbene units, again proving the beneficial influence of carbene ligands on the MLCT lifetime [32]. This longer excited state lifetime could increase the chance for an electron transfer process to take place, either from the iron carbene PS to the Pt nanoparticle (= oxidative quenching) or from the sacrificial electron donor to the PS (= reductive quenching). However, as the overall performance of the FeNHC sensitizers is low and no mechanistic investigations were presented, it is quite speculative to correlate the slight difference in TON to any of the molecular properties.

$[\text{Fe}(\text{bpymi})(\text{pbdppi})]^{2+}$ (Figure 8) is a heteroleptic complex featuring the bpy-NHC ligand bpymi and the CNC ligand pbdppi, resulting in the coordination of three NHC moieties to the iron center [32]. This should lead to a stronger destabilization of e_g^* orbitals than in the previously mentioned complexes with one tpy-type ligand and one CNC ligand while still providing rather low-lying π^* levels through the bpy moiety. Indeed, $[\text{Fe}(\text{bpymi})(\text{pbdppi})]^{2+}$ shows a combination of rather beneficial properties. MLCT absorption bands appear in a broad window between 350 and 550 nm with attenuation coefficients of $5000 \text{ to } 6000 \text{ M}^{-1} \text{ cm}^{-1}$. The combination of three NHC moieties and the bpy-type ligand seems to lead to a sufficient destabilization of MC states and stabilization of MLCT states to push the $^3\text{MLCT}$ lifetime out of the fs regime to 3.6 ps. Assignment of the states was concluded from TA spectroscopic measurements supported by X-ray techniques and DFT calculations [32].

An extension to the above mentioned pytpy complexes was recently reported [32]. In this study the pytpy ligand in $[\text{Fe}(\text{pbdppi})(\text{pytpy})]^{2+}$ was modified by methylation or attachment of a chloro-bis(dimethylglyoximate)-cobalt(III) ($\text{CoCl}(\text{dmg})_2$) unit (Figure 9), yielding $[\text{Fe}(\text{pbdppi})(\text{pytpyMe})]^{3+}$ and $[\text{Fe}(\text{pbdppi})(\text{pytpyCoCl}(\text{dmg})_2)]^{2+}$ (Fe-Co), respectively. Similar to $[\text{Fe}(\text{pbhi})(\text{pytpy})]^{2+}$, steady state absorption of $[\text{Fe}(\text{pbdppi})(\text{pytpy})]^{2+}$ shows two MLCT bands at 515 and 553 nm. Methylation of the pytpy unit leads to a further bathochromic shift of 20–30 nm of these bands, while the introduction of the $\text{CoCl}(\text{dmg})_2$ fragment only leads to a shift of 5 nm. The bathochromic shift indicates that the π^* LUMO level is lowered more significantly than the t_{2g} orbitals by the modifications made. As evident from the crystal structures determined by X-ray diffraction analysis, the torsion angle between the tpy and py moiety in the methylated compound is much smaller than in Fe-Co (8° vs. 38°). This leads to better communication along the π system for $[\text{Fe}(\text{pbdppi})(\text{pytpyMe})]^{3+}$ compared to Fe-Co which explains the more pronounced bathochromic shift

of the MLCT absorption bands [32]. Fe-Co represents an interesting step towards a noble metal-free photosensitizer-reduction catalyst-assembly. However, little communication between the metal centers was found which leads to the suspicion that Fe-Co would not make a very powerful photocatalyst in light-driven proton reduction, but no investigations in this direction have been presented so far.

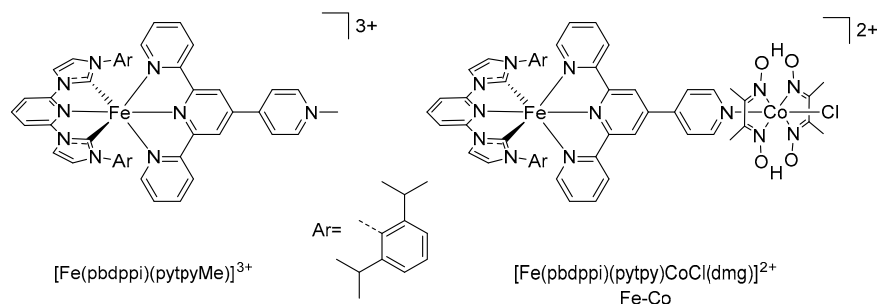


Figure 9. Heteroleptic FeNHC-pytpy complexes modified by methylation or introduction of a $\text{CoCl}(\text{dmg})_2$ unit leading to hetero-bimetallic compound Fe-Co [36].

A theoretical study calculating NTOs by (TD-)DFT methods investigated the effect of connecting an anthracene unit to the para-position of one of the pyridine rings of a $[\text{Fe}(\text{pbmi})_2]^{2+}$ core by different linker motifs [37]. Direct connection and different aliphatic and ethynyl-based linkers were examined (Figure 10). For the ethynyl bridged structures, a planar arrangement of the ligand and anthracene unit was found, while for all other types of connections the anthracene unit is not parallel to the ligand it is connected to. For these latter complexes, only a small influence on the absorption properties was predicted, while for the ethynyl bridged, a new very strong absorption feature appears in the red part of the spectrum. It is expected that the conjugated connection to the anthracene π system would lead to “long-range MLCT” transitions where electron density is redistributed from the metal center to the anthracene moiety in the excited state. The energy of the lowest triplet excited state was predicted to lie below the MC states, which could lead to a long excited state lifetime of CT character with the anthracene unit functioning as an energy reservoir [37]. Despite these interesting predictions, no synthetic realization of these compounds has been reported to date.

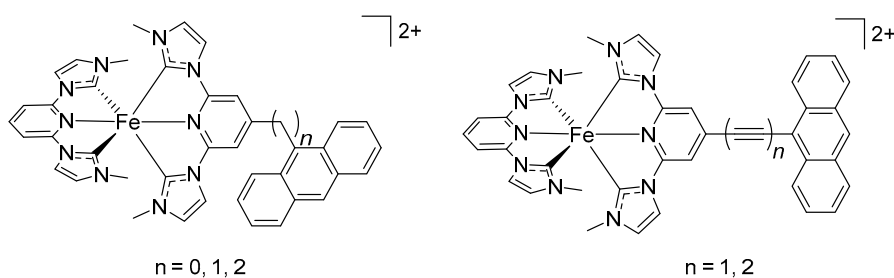


Figure 10. FeNHC complexes of connected to an anthracene unit via different linker motifs [37].

3.3. FeNHC Complexes with Meridional Tridentate Ligands with Anchoring Groups

3.3.1. Homoleptic FeNHC Complexes with Anchoring Groups

Research on DSSCs utilizing iron complexes as PSs was initiated in the late nineties using $[\text{Fe}(\text{bpydc})_2(\text{CN})_2]$ (bpydc = (2,2'-bipyridine-4,4'-dicarboxylic acid) and related iron(II) complexes [38,39] and has been a topic of discussion since [40]. However, the discovery of the promising photoproperties of $[\text{Fe}(\text{pbmi})_2]^{2+}$ spurred further research in this direction. In 2015, two studies on a complex containing anchoring groups, $[\text{Fe}(\text{cpbmi})_2]^{2+}$ (cpbmi = (carboxypyridine-2,6-diyl)bis(1-methyl-imidazol-2-ylidene) (Figure 11a), appeared [22,23]. Introduction of the carboxylic acid group brings some beneficial influences: the low-energy MLCT band in the absorption spectrum

is bathochromically shifted in a significant manner from 460 to 520 nm for $[\text{Fe}(\text{pbmi})_2]^{2+}$ and $[\text{Fe}(\text{cpbmi})_2]^{2+}$, respectively. This bathochromic shift can be rationalized by the electron withdrawing character of the carboxylic acid group that leads to a lowering of the LUMO energy which is also reflected in an anodic shift of the ligand-based reduction potential in CV (-1.95 and -1.35 V vs. SCE, -2.34 and -1.74 vs. Fc^+/Fc for $[\text{Fe}(\text{pbmi})_2]^{2+}$ and $[\text{Fe}(\text{cpbmi})_2]^{2+}$, respectively) [22]. Most notably, for $[\text{Fe}(\text{cpbmi})_2]^{2+}$ the $^3\text{MLCT}$ lifetime was found to be 16.5 ps and is thus almost twice as long as for the $[\text{Fe}(\text{pbmi})_2]^{2+}$ congener. (TD-)DFT calculations of the NTOs showed significant delocalization of the excited state over the carboxylic acid group, which is considered beneficial for electron injection of the surface-immobilized dye. Taking the above-mentioned reduction potentials as an estimate, electron injection into a TiO_2 semiconductor surface (-0.7 V vs. SCE, -1.1 V vs. Fc^+/Fc) from the excited state should be well feasible for $[\text{Fe}(\text{cpbmi})_2]^{2+}$. Furthermore, recovery of the then oxidized dye by redox mediator I_3^-/I^- (0.2 V vs. SCE, -0.2 V vs. Fc^+/Fc) can be expected considering the potential of $\text{Fe}(\text{III}/\text{II})$ couple of 0.85 V vs. SCE (0.46 V vs. Fc^+/Fc) (Figure 11b). However, the first assembled DSSC using $[\text{Fe}(\text{cpbmi})_2]^{2+}$ as the dye showed very low overall solar-to-current efficiency of 0.13% [22].

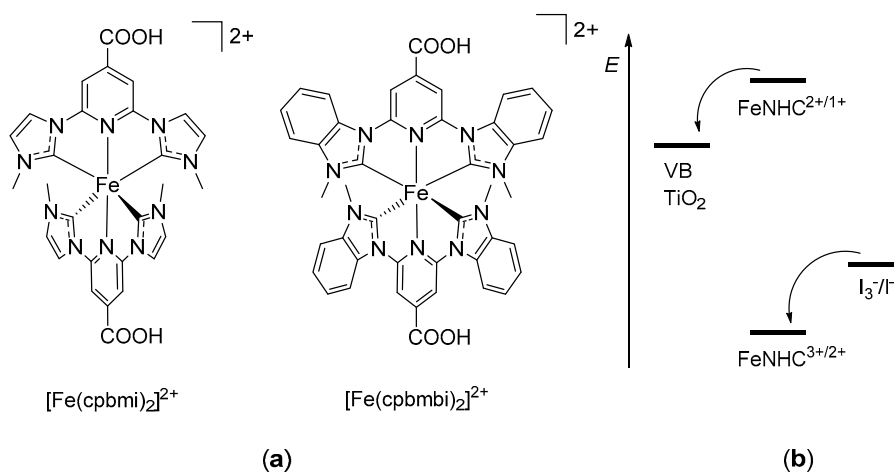


Figure 11. (a) FeNHC complexes with anchoring groups for surface sensitization [22,23,33]. (b) Schematic presentation of electron transfer processes in a dye-sensitized solar cells (DSSC) utilizing, e.g., $[\text{Fe}(\text{cpbmi})_2]^{2+}$ as a dye.

Nevertheless, very fast and efficient electron injection into TiO_2 nanoparticles (NP) was proven by a range of spectroscopic investigations in another study [23]: the combination of TA-, electron paramagnetic resonance- (EPR) and terahertz spectroscopy revealed, that electrons are injected with 92% efficiency on a 3.1 ps timescale. However, under the applied conditions only 13% of the injected electrons remain in the semiconductor for more than 10 ns while the rest undergoes recombination with the oxidized dye within a few hundred ps [23]. In an extensive computational study, different methods were used to calculate orbital energies and the excited state landscape of $[\text{Fe}(\text{cpbmi})_2]^{2+}$ and some related complexes [41]. The results are in agreement with the spectroscopic findings and explain well the extended excited state lifetime of $[\text{Fe}(\text{cpbmi})_2]^{2+}$ compared to $[\text{Fe}(\text{pbmi})_2]^{2+}$ and also electron injection into TiO_2 was predicted to be feasible [41]. A possible reason for the low efficiency of the DSSC sensitized with $[\text{Fe}(\text{cpbmi})_2]^{2+}$ was postulated to be the non-ideal localization of the LUMO for the surface bound dye [42]. Calculations showed that the LUMO is mostly localized on the ligand and anchoring group that are not involved in the surface binding, which makes injection from the lowest MLCT state unfavorable. In contrast, the LUMO+1 level is mainly localized on the bound anchoring group and semiconductor nanocluster. This can be rationalized as follows: when TiO_2 is bound to the anchoring group, it forms a less strong electron acceptor than the proton of the non-anchoring carboxylic acid group. The LUMO/LUMO+1 localization could thus be inverted by deprotonation of the free $-\text{COOH}$ group. However, in practice this would facilitate desorption of the dye from the semiconductor

surface, therefore the use of heteroleptic complexes was suggested instead (c.f., Section 3.3.2) [42]. It should be stated that DSSCs are a multicomponent system and variation of different constituents and the manufacturing process can have a significant influence on the performance of the assembled cell. In recent studies DSSCs with up to 0.57% and later 0.66% efficiency were realized using $[\text{Fe}(\text{cpbmi})_2]^{2+}$ as PS and I_3^-/I^- as redox mediator but employing a co-adsorbent and systematically varying the solvent, an ionic liquid additive and further additives [43,44]. Very recently, the efficiency of DSSCs employing $[\text{Fe}(\text{cpbmi})_2]^{2+}$ as a dye was pushed even higher to just above 0.9%, using an I_3^-/I^- electrolyte with guanidinium thiocyanate and other additives on carefully manufactured semiconductor surfaces [45]. The study also came to the conclusion that the main problems leading to the still rather low overall efficiencies are the recombination of injected electrons with oxidized electrolyte molecules and the competing fast deactivation of the excited state [45].

As longer (CT) excited state lifetimes also prolong the time for possible electron injection into a semiconductor surface, it was reasoned that the complex $[\text{Fe}(\text{cpbmbi})_2]^{2+}$ ((cpbmbi = (carboxypyridine-2,6-diyl)bis(1-methyl-benzimidazol-2-ylidene)) (Figure 11a) should be a better sensitizer [32]. As discussed above, the introduction of the carboxylic acid groups leads to stabilization of the MLCT states becoming apparent by a bathochromic shift of the low-energy MLCT absorption band (440 to 501 nm) and extension of the $^3\text{MLCT}$ lifetime from 16.4 to 26 ps in comparison to $[\text{Fe}(\text{pbmbi})_2]^{2+}$ [33]. Indeed, quantum chemical (QC) investigations predicted that in the case of $[\text{Fe}(\text{cpbmbi})_2]^{2+}$ the ^3MC state is by 0.12 eV higher in energy than the $^3\text{MLCT}$ state. However, due to the small barrier, the ^3MC state is still thermally accessible explaining the deactivation of the $^3\text{MLCT}$ state on a ps timescale. Despite these promising properties, DSSCs sensitized with $[\text{Fe}(\text{cpbmbi})_2]^{2+}$ showed poor performance with an efficiency of 0.03%. These cells show a very low short circuit current (I_{SC}) of 0.12 mA cm^{-2} even when compared to $[\text{Fe}(\text{cpbmi})_2]^{2+}$ ($I_{\text{SC}} = 0.41 \text{ mA cm}^{-2}$), which points to insufficient interfacial charge separation and/or fast charge recombination [42].

3.3.2. Heteroleptic FeNHC Complexes with Anchoring Groups

In order to avoid the non-optimal localization of HOMOs and LUMOs of adsorbed homoleptic dyes containing free anchoring groups as outlined above, heteroleptic complexes were suggested as a solution. The most straightforward modification is $[\text{Fe}(\text{cpbmi})(\text{pbmi})]^{2+}$ where only one of the CNC ligands has an anchoring group. This compound was presented together with $[\text{Fe}(\text{cpbai})(\text{pbmi})]^{2+}$ (cpbai = (carboxypyridine-2,6-diyl)bis(1-*p*-anisyl-imidazol-2-ylidene)) and $[\text{Fe}(\text{cpbdpai})(\text{pbmi})]^{2+}$ (cpbdpai = (carboxypyridine-2,6-diyl)bis(1-*N,N*-diphenylaniliny-imidazol-2-ylidene)) and the structures are shown in Figure 12 [42].

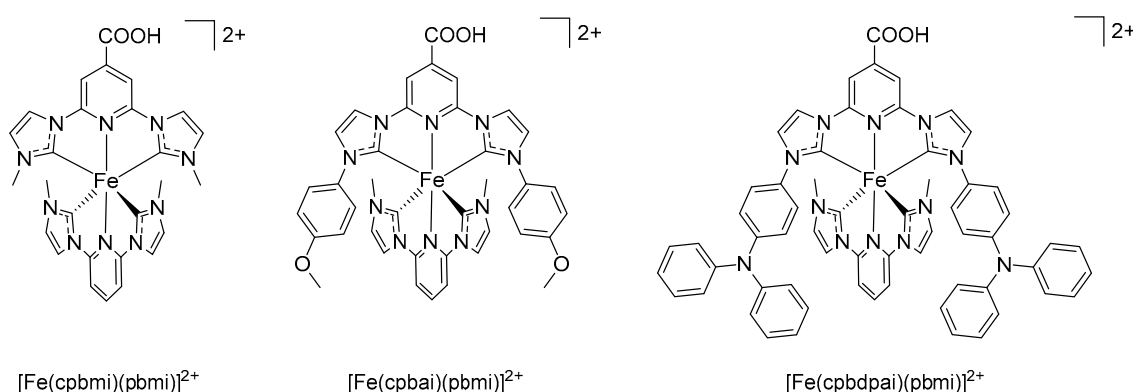


Figure 12. Heteroleptic FeNHC complexes with anchoring groups for surface sensitization [42].

The properties of these heteroleptic complexes are quite similar. The low-energy MLCT band appears around 510 nm ($\epsilon = 9500\text{--}17700 \text{ M}^{-1} \text{ cm}^{-1}$) and the Fe(III/II) redox couple at around 0.8 V (vs. SCE, ca 0.4 V vs. Fc^+/Fc), typical for tetra-carbene CNC complexes. Furthermore, their $^3\text{MLCT}$

excited state lifetimes were found to be between 10 and 14 ps and are thus close to those of the parent dicarboxylic complex $[\text{Fe}(\text{cpbmi})_2]^{2+}$ [22,23,42]. Still, their heteroleptic design holds promise to facilitate directional electron transfer towards the anchoring group upon photoexcitation: the electron donating substituents on $[\text{Fe}(\text{cpbai})(\text{pbmi})]^{2+}$ and $[\text{Fe}(\text{cpbdpai})(\text{pbmi})]^{2+}$ should help to accommodate the hole in the excited state far away from the semiconductor surface and thus hinder recombination. However, the efficiency of DSSCs sensitized with these dyes was found to be low with only around 0.1%. While the loading and attenuation coefficients of these dyes are comparable to the Ru reference dye N719, the most striking difference are the very low I_{SC} values of around 0.35 mA cm^{-2} compared to 13.25 mA cm^{-2} for N719. QC investigations led to the conclusion that electron injection of the heteroleptic PSs happens on the same timescale as the deactivation of the $^3\text{MLCT}$ state, which is detrimental for efficient electron injection. Further, fast recombination of the injected electron with both, oxidized dye and the redox mediator seems to take place, explaining the low efficiency of the cells [42]. For more detailed discussions on DSSCs incorporating Fe compounds, the reader is also referred to the recent literature on this topic [46,47].

4. FeNHC Complexes with Bidentate Ligands

The use of tridentate meridional coordinating ligands like tpy or the above-mentioned CNC ligands do often not provide an ideal (octahedral) coordination geometry. In the parent $[\text{Fe}(\text{pbmi})_2]^{2+}$, for instance, the angles of *trans*-standing coordinating atoms are only good for the N-atoms (178.6°) while the C–Fe–C angles are around 158° as determined by X-ray crystallography analysis [21]. This leads to non-ideal overlap of the ligand and metal orbitals, resulting in a weaker than possible ligand field splitting. The *trans*-angles can be easily improved by using bidentate ligands as these can arrange themselves more freely around the metal center.

An example of an iron complex making use of bidentate ligands is $[\text{Fe}(\text{bpy})(\text{btz})_2]^{2+}$ (btz = 4,4'-bis(1,2,3-triazol-5-ylidene) (Figure 13) presented in 2015 [48], containing four NHC moieties. The reasoning behind the design of the complex was to influence MLCT as well as MC states in a beneficial manner: use of the bpy ligand should provide low-lying π^* orbitals to accommodate the electron in the excited state and the btz ligand, incorporating strongly σ -donating mesoionic carbene motifs, should destabilize the e_g^* while the better π -accepting character of mesoionic carbenes should lead to a stabilization of the t_{2g} orbitals. In this way, the excited state should also be localized on only one side of the complex initiating directional electron transfer leading to a final charge-separated state, which could be beneficial for future sensitization or photocatalytic applications.

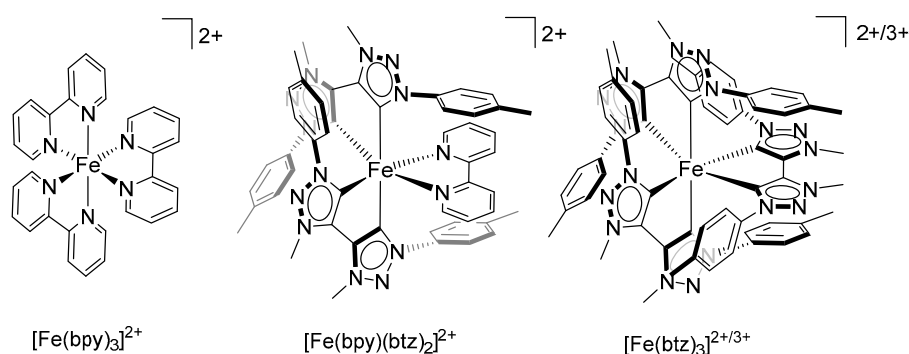


Figure 13. Prototype $[\text{Fe}(\text{bpy})_3]^{2+}$ and FeNHC complexes incorporating the mesoionic btz ligand [48–50].

The crystal structure of $[\text{Fe}(\text{bpy})(\text{btz})_2]^{2+}$ reveals C–Fe–C *trans*-angles of 172° – 178° , which is indeed a lot closer to the ideal 180° compared to the $\sim 160^\circ$ C–Fe–C *trans*-angles of complexes bearing the CNC-ligands mentioned above [48]. The Fe(III/II) redox couple in $[\text{Fe}(\text{bpy})(\text{btz})_2]^{2+}$ appears at -0.35 V (vs. Fc^+/Fc) and is dramatically shifted compared to that of $[\text{Fe}(\text{bpy})_3]^{2+}$ at 0.68 V (vs. Fc^+/Fc)

but also significantly more cathodic than that of other FeNHC complexes such as parental $[\text{Fe}(\text{pbmi})_2]^{2+}$ with the same number of carbene donors (around 0.4 V vs. Fc^+/Fc). Thus, it seems that the stabilization of the t_{2g} levels is smaller than anticipated even though the orbital energies of bpy and btz seem to be very similar: electrochemical investigations showed three reduction signals for $[\text{Fe}(\text{bpy})(\text{btz})_2]^{2+}$ in close vicinity to each other indicating that the π^* orbitals of btz are just a little higher in energy compared to bpy. The first ligand reduction (associated to reduction of bpy) is less severely shifted than the Fe(III/II) couple, comparing $[\text{Fe}(\text{bpy})_3]^{2+}$ and $[\text{Fe}(\text{bpy})(\text{btz})_2]^{2+}$ (−1.75 to −2.28 vs. Fc^+/Fc) leading to a smaller electrochemical bandgap for $[\text{Fe}(\text{bpy})(\text{btz})_2]^{2+}$. This is also obvious from steady state absorption spectroscopy: the lowest-energy MLCT band is shifted bathochromically from 520 nm in $[\text{Fe}(\text{bpy})_3]^{2+}$ to 609 nm in $[\text{Fe}(\text{bpy})(\text{btz})_2]^{2+}$. The $^3\text{MLCT}$ lifetime was estimated by TA spectroscopy to be 13 ps for $[\text{Fe}(\text{bpy})(\text{btz})_2]^{2+}$ which is an increase by two orders of magnitude compared to the 130 fs $^3\text{MLCT}$ lifetime of $[\text{Fe}(\text{bpy})_3]^{2+}$. Detailed spectroelectrochemical (SEC) investigations and (TD-)DFT computations corroborated the assignment of the 13 ps lifetime to the decay of the $^3\text{MLCT}$ state. Further support for this also comes from comparison of X-ray spectroscopic data of related $[\text{Fe}(\text{bpy})(\text{CN})_4]^{2-}$ [48]. Recently, time-resolved X-ray investigations revealed a more complex decay mechanism for $[\text{Fe}(\text{bpy})(\text{btz})_2]^{2+}$ and found a lifetime of around 8 ps for the $^3\text{MLCT}$ state (when excited at shorter wavelengths compared to earlier studies) [51].

If an iron center is saturated with mesoionic NHC donors by ligation of three btz ligands leading to $[\text{Fe}(\text{btz})_3]^{n+}$ (Figure 13), the Fe(III/II) couple is shifted to even more negative values (−0.58 V vs. Fc^+/Fc) compared to $[\text{Fe}(\text{bpy})(\text{btz})_2]^{2+}$ (−0.35 V vs. Fc^+/Fc) [48,50]. This results in the iron center being in the Fe(III) oxidation state under ambient conditions. The electronic configuration of $[\text{Fe}(\text{btz})_3]^{3+}$ was investigated by a range of electron spin sensitive methods proving that there are five electrons in the t_{2g} orbitals, instead of six and one ligand being internally oxidized to the radical cation. As there is a vacancy in the t_{2g} orbitals, the lowest energy transitions are excitations from the ligand π orbitals to the metal center as illustrated in Figure 14. The corresponding LMCT bands are located at 528 and 558 nm, however, with rather low attenuation coefficients of around $1500 \text{ M}^{-1} \text{ cm}^{-1}$.

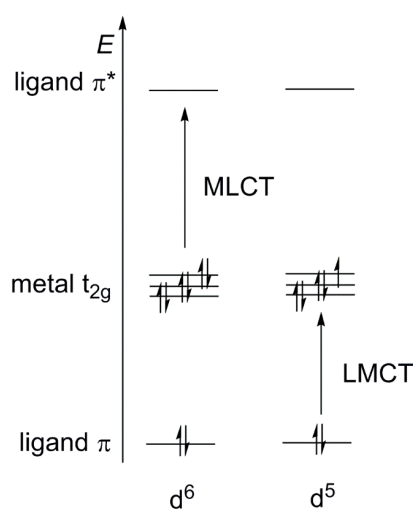


Figure 14. Typical excitation processes in d^6 and d^5 observed for FeNHC complexes.

Importantly, $[\text{Fe}(\text{btz})_3]^{3+}$ was the first iron complex to show photoluminescence in fluid solution at room temperature. The emission maximum is located at 600 nm and thus being very close to the LMCT absorption band at 558 nm. Due to the small energetic difference (0.15 eV) between these bands the luminescence feature was assigned to stem from the spin allowed transition from the $^2\text{LMCT}$ state to the doublet ground state (^2GS). This is in contrast to the Fe(II) d^6 complexes, where the long-lived CT state is a $^3\text{MLCT}$ state that is populated by intersystem crossing from the initially populated $^1\text{MLCT}$ state. Time-resolved optical spectroscopy revealed that the transient absorption- as well as the transient photoluminescence spectra decay with the same kinetics and a long lifetime of around

100 ps was established with both techniques. The LMCT character of this state was further proven by the transient absorption features that resemble those of the electrochemically accessed (ground state) Fe(II) complex. QC calculations suggested that the ^4MC and ^6MC states, that could facilitate fast radiationless deactivation, are destabilized and pushed away on the reaction coordinate in analogy to the ^3MC and ^5MC states in the Fe(II) d^6 complexes discussed earlier. Thus it seems that the strategy of destabilizing MC states by strong σ donors is more universally applicable [50], as demonstrated here, not only for prolonging the lifetime of MLCT states but also for LMCT states of Fe(II) and Fe(III) complexes, respectively. More detailed investigations by hard X-ray absorption spectroscopic methods and (TD-)DFT calculations on $[\text{Fe}(\text{btz})_3]^{3+}$ corroborated the strong interaction between the metal center and the carbene ligands leading to strong ligand field splitting [52]. The energy difference between the t_{2g} and e_g^* orbitals was estimated to be 2 to 3 eV, which solidifies the interpretation that MC states can be significantly destabilized by strongly σ -donating carbene ligands [52].

The corresponding Fe(II) complex $[\text{Fe}(\text{btz})_3]^{2+}$ can not only be electrochemically generated but can also be accessed by chemical reduction with sodium dithionate and the resulting compound was isolated and fully characterized [49]. The compound is stable in the solid state and in deaerated acetonitrile solution. While the structure of the compound is very similar in both oxidation states as demonstrated by X-ray diffraction analysis, the absorption bands of $[\text{Fe}(\text{btz})_3]^{2+}$ are significantly stronger than those of $[\text{Fe}(\text{btz})_3]^{3+}$: lower-energy bands with maxima at 540 and 730 nm were assigned to MLCT transitions into different π^* levels of btz, showing attenuation coefficients between 2500 and 5500 $\text{M}^{-1} \text{cm}^{-1}$. The assignment to MLCT transitions was corroborated by SEC investigations and DFT calculations. TA spectroscopic measurements led to the conclusion that the $^3\text{MLCT}$ state has an impressive lifetime of 528 ps. The increase in CT excited state lifetime from 100 ps in $[\text{Fe}(\text{btz})_3]^{3+}$ to more than 500 ps in $[\text{Fe}(\text{btz})_3]^{2+}$ can be rationalized by the spin-forbidden transition to the ground state from a $^3\text{MLCT}$ to the singlet ground state in the latter compound, compared to the spin-allowed decay from a $^2\text{LMCT}$ to the doublet ground state in the former. The existence of long-lived CT states in different oxidation states of the same compound is interesting as the excited state of $[\text{Fe}(\text{btz})_3]^{2+}$ is a strong reductant (-1.6 V vs. Fc^+/Fc) and the excited state of $[\text{Fe}(\text{btz})_3]^{3+}$ is a strong oxidant (1.5 V vs. Fc^+/Fc) which could be interesting for future application in tandem devices, e.g., DSSCs using both, n-type and p-type semiconductors, and PSs based on the same iron complex. In that regard it is interesting to note that excitation of $[\text{Fe}(\text{btz})_3]^{2+}$ at different wavelengths resulted in a change of the excited state dynamics and influences some of the decay components [53]. Most importantly, however, the 500 ps lifetime was found in all experiments, indicating that broadband excitation, e.g., by sunlight should still result in same long-lived excited state without dramatically changing the efficiency of its generation [53].

The use of a bidentate pyridine-imidazole-derived ligand led to $[\text{Fe}(\text{mpi})_3]^{2+}$ (mpi = 3-methyl-1-(pyridin-2-yl)-imidazol-2-ylidene) which exists in two different isomers with either meridional or facial coordination of the carbene/pyridine moieties (Figure 15) [54]. When synthesized the complex is obtained in a 14:1 *mer/fac* mixture that is inseparable. The steady state absorption spectrum of the mixture shows a strong band at 430 nm and a less intense feature at 360 nm. QC calculations suggested that both isomers are low-spin in their ground state and the low-energy absorption band was assigned to have MLCT character while the higher-energy transition has marked MC character. More extensive computational investigations led to further predictions: after excitation of either isomer of $[\text{Fe}(\text{mpi})_3]^{2+}$ from the S_0 ground state an ultrafast decay to a manifold of three triplet states (T_{1-3}) at the Franck–Condon vicinity (i.e., without significant structural changes) takes place. Further decay will be dictated by these states of mixed MLCT/MC nature. Progression of these states along the reaction coordinate leads to an increase of the MC character, resulting in the elongation of (mainly) one of the Fe–N bonds. For the *fac*-isomer, this elongation can lead to a bond length up to 3.5 Å resulting in a strong increase of the S_0 energy, which leads to a singlet-triplet crossing. This crossing, accompanied by Fe–N bond dissociation, is postulated to be the main deactivation channel for the *fac*-isomer. For *mer*- $[\text{Fe}(\text{mpi})_3]^{2+}$ the minimum of the T_1 potential energy surface (PES) lies at around

2.8 Å Fe–N distance and is lower in energy compared to the *fac*-isomer (1.13 vs. 1.36 eV) which points to faster vibrational relaxation from the triplet state for the *mer*-compound. Quintet states were found to play a minor role in the deactivation of $[\text{Fe}(\text{mpi})_3]^{2+}$ as they are too high in energy to be efficiently accessed [54].

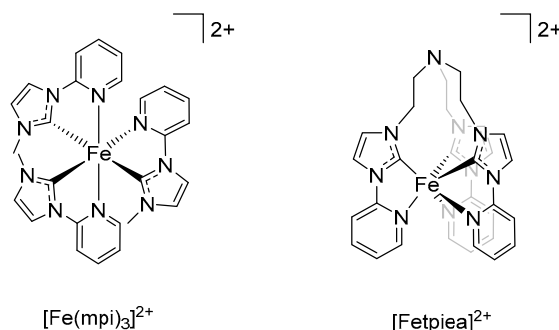


Figure 15. *mer*- $[\text{Fe}(\text{mpi})_3]^{2+}$ and analogue with forced facial coordination [54,55].

In order to give experimental proof to the above made predictions $[\text{Fe}(\text{mpi})_3]^{2+}$ and $[\text{Fetpiea}]^{2+}$ (*tpiea* = tris(2-(1-(pyridin-2-yl)-imidazol-2-ylidene)ethyl)amine) (Figure 15) were investigated by TA spectroscopy in detail [55]. The *tpiea* ligand is a six-fold coordinating hemi-cage ligand featuring the same coordination sites as three *mpi* ligands, therefore, this ligand is discussed here in this chapter. Its use leads to a facial coordination of the different donor moieties to the metal, allowing for the best possible comparison of the *fac*- and *mer*-isomers of iron complexes with three pyridine and three imidazolylidene coordination moieties. Steady state absorption spectroscopy shows bands at 369 and 438 nm for $[\text{Fetpiea}]^{2+}$ which is close to those of $[\text{Fe}(\text{mpi})_3]^{2+}$ (360 and 430 nm) but slightly bathochromically shifted. Compared to parental $[\text{Fe}(\text{pbmi})_2]^{2+}$, the absorption bands of both, $[\text{Fetpiea}]^{2+}$ and $[\text{Fe}(\text{mpi})_3]^{2+}$ are hypsochromically shifted, indicating a larger HOMO–LUMO gap. Interestingly, the Fe(III/II) couple is slightly cathodically shifted for $[\text{Fe}(\text{mpi})_3]^{2+}$ (0.65 V vs. SCE, 0.26 V vs. Fc^+/Fc) and $[\text{Fetpiea}]^{2+}$ (0.61 V vs. SCE, 0.24 V vs. Fc^+/Fc) compared to $[\text{Fe}(\text{pbmi})_2]^{2+}$ (0.71 V vs. SCE, 0.28 vs. Fc^+/Fc) [55]. It can be hypothesized that the HOMO level is slightly destabilized in the pyridine-imidazolylidene complexes even though they contain one carbene moiety less than, e.g., $[\text{Fe}(\text{pbmi})_2]^{2+}$. So, apparently the π -accepting properties of the bidentate pyridine-imidazolylidene ligands used in this study are worse than in the *pbmi* ligand, possibly due to the smaller π system of the bidentate pyridine-imidazolylidene-based ligands. This would also explain the higher lying π^* orbitals of these ligands and thus also the overall hypsochromically shifted MLCT absorptions. However, this is not reflected in the electrochemical data, that predicts a somewhat smaller electrochemical bandgap (0.1–0.15 V) for $[\text{Fe}(\text{mpi})_3]^{2+}$ and $[\text{Fetpiea}]^{2+}$ compared to parental $[\text{Fe}(\text{pbmi})_2]^{2+}$. Computational investigations confirmed that the excited state landscape of $[\text{Fetpiea}]^{2+}$ is qualitatively similar to that of *fac*- $[\text{Fe}(\text{mpi})_3]^{2+}$. Detailed TA spectroscopic measurements found three components for the decay of the excited state with lifetimes of $\tau_1 = 0.3\text{--}0.5$ ps, $\tau_2 = 3\text{--}4$ ps and $\tau_3 = 15\text{--}20$ ps for $[\text{Fetpiea}]^{2+}$. From the obtained data it was concluded that rather than a sequential decay involving three states that are populated one after another, a parallel decay takes place from two states that are populated from the initially excited state. Similar behaviour was suggested for $[\text{Fe}(\text{mpi})_3]^{2+}$ with lifetimes of $\tau_1 = 0.2\text{--}0.5$ ps, $\tau_2 = 2\text{--}3$ ps and $\tau_3 = 15\text{--}20$ ps. The shorter lifetime τ_2 for $[\text{Fe}(\text{mpi})_3]^{2+}$ was explained by the excited state landscape of *mer*- $[\text{Fe}(\text{mpi})_3]^{2+}$ (which is the dominant species also in the TA spectroscopic experiments) that facilitates faster deactivation as described above. Overall, these findings show that the excited state dynamics can be more complex for FeNHC complexes than often initially considered and also that isomerism/symmetry can have a pronounced influence on excited state dynamics. This needs to be taken into account for the development and investigation of new generations of FeNHC complexes.

5. FeNHC Complex with Facial Coordinating Tridentate Ligand

The coordination of a tridentate ligand can also occur in a facial manner when a tripodal, or “scorpionate”, backbone is used instead of the meridional structure of the CNC ligands discussed above. An example for this is the phtmib (phtmib = phenyl(tris(3-methylimidazol-2-ylidene))borate) ligand (Figure 16), which is a modification of the earlier reported htmib (hydro(tris(3-methylimidazol-2-ylidene))borate) ligand bearing a phenyl group instead of hydrogen as a fourth substituent on the boron atom [56,57]. The negatively charged boron atom of the ligand increases the electron density on the ligand making it an even stronger σ donor [58]. As the ligand also provides a nearly perfect octahedral coordination geometry around the metal center it is assumed to induce a very strong ligand field splitting [59]. An iron complex making use of this ligand has recently been synthesized and investigated (Figure 16) [60]. Even though an iron complex based on htmib was reported earlier, it was never investigated photophysically [57].

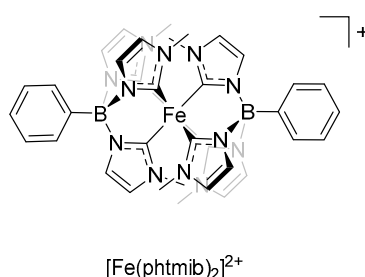


Figure 16. Complex incorporating a Fe(III) center coordinated by two phtmib ligands [60].

Due to the strongly σ -donating character of the ligands, the t_{2g} orbitals are significantly pushed up in energy leading to a strong cathodic shift of the Fe(III/II) couple to -1.16 V (vs. Fc^+/Fc , compared to -0.58 V for $[Fe(btz)_3]^{n+}$ [50]) so that under ambient conditions the complex is in the Fe(III) oxidation state. This leads to a d^5 electron configuration and thus a vacancy on one of the t_{2g} orbitals as explained for $[Fe(btz)_3]^{3+}$ (c.f., Section 4 and Figure 14). As the π^* orbitals of the ligand are also very high in energy, the lowest energy transition is a spin-allowed LMCT from the ligand π orbitals to the Fe(III) center peaking at 502 nm ($\epsilon = 2950$ M⁻¹ cm⁻¹) similar to the previously discussed $[Fe(btz)_3]^{3+}$. Remarkably, $[Fe(phtmib)_2]^+$ shows visible emission at 655 nm in MeCN solution at room temperature with a quantum yield of 2.1%, as high as for $[Ru(bpy)_3]^{2+}$. The excited state lifetime of the ²LMCT state was determined to be impressive 1.96 ns by TA- and time-resolved photoluminescence spectroscopic measurements, four times longer than for $[Ru(tpy)_2]^{2+}$. Furthermore, the excited state redox potentials of -1.9 and 1.0 V (vs. Fc^+/Fc) outperform those of $[Ru(bpy)_3]^{2+}$ (-0.86 and 0.84 V vs. SCE, -1.25 and 0.45 V vs. Fc^+/Fc) [6]. With these outstanding photophysical properties, $[Fe(phtmib)_2]^+$ is a very promising candidate for photocatalytic and (when appropriately functionalized) photovoltaic applications. Indeed, in bimolecular quenching experiments oxidative as well as reductive quenching with methylviologen and diphenylamine, respectively, was found to be feasible [60].

6. Synthetic Approaches to FeNHC Complexes

6.1. Synthesis of Homoleptic Complexes

While the synthesis of homoleptic iron polypyridyl complexes can be fairly simple and often just requires mixing of ligand and iron precursor in a solvent, the synthesis of NHC containing complexes is more challenging. To be able to coordinate the carbene precursor to the metal center, deprotonation of imidazolium type precursors is necessary and the so created carbene is a reactive species that can undergo reactions with CO_2 , H_2O , O_2 or dimerize which makes it mandatory to work under dry and inert conditions and sometimes at low temperatures [61].

Homoleptic FeNHC complexes are rather straightforward to synthesize if the necessary precautions are taken, however, purification can be cumbersome. Preparation of complexes of the type $[\text{Fe}(\text{pbRi})_2]^{2+}$ (R = alkyl substituent, see Figure 17) can be roughly divided into two different procedures using either DMF (*N,N*-dimethylformamide) or THF (tetrahydrofuran) as solvent. The procedure in THF was used in the first report on parental $[\text{Fe}(\text{pbmi})_2]^{2+}$ and $[\text{Fe}(\text{pbbi})_2]^{2+}$: a suspension of the ligand in THF was cooled to -78 °C before addition of the base (freshly prepared $\text{KO}t\text{Bu}$ in THF), followed by the addition of a solution of dry FeBr_2 in THF. The reaction mixture was then allowed to warm to RT (room temperature) and was stirred overnight. After filtration and solvent removal, the crude product was precipitated from aqueous solution as the hexafluorophosphate salt. Subsequently, size-exclusion column chromatography was performed to give the pure product after reprecipitation 53% and 55% yield for $[\text{Fe}(\text{pbmi})_2]^{2+}$ and $[\text{Fe}(\text{pbbi})_2]^{2+}$, respectively. The bulkier *t*Bu groups in pbbi were considered to hinder dimerization of the ligand; however, the yield is only marginally higher than for Me-substituted pbmi [21]. Essentially, the same synthetic and purification procedure was also applied for the synthesis of $[\text{Fe}(\text{btz})_3]^{n+}$ ($n = 2-3$) and $[\text{Fe}(\text{phtmib})_2]^+$ with yields of around 40% [49,50,60]. A similar strategy with THF as solvent was used to synthesize $[\text{Fe}(\text{pbpi})_2]^{2+}$ and $[\text{Fe}(\text{bpyimi})_2]^{2+}$ employing less cold conditions (-10 and -18 °C, respectively) and using $\text{LiN}(\text{SiMe}_3)_2$ as the base and subsequent addition of a FeBr_2 solution [24,32]. For $[\text{Fe}(\text{pbpi})_2]^{2+}$ the crude product was filtered off, dried, and recrystallized in about 85% yield as the bromide salt. The counterion can be easily exchanged to hexafluorophosphate by treatment with NH_4PF_6 in aqueous solution [24]. The crude of $[\text{Fe}(\text{bpyimi})_2]^{2+}$ was dried after overnight reaction and then reprecipitated from aqueous solution by addition of NH_4PF_6 . Subsequently, the precipitate was recrystallized in 84% yield [32].

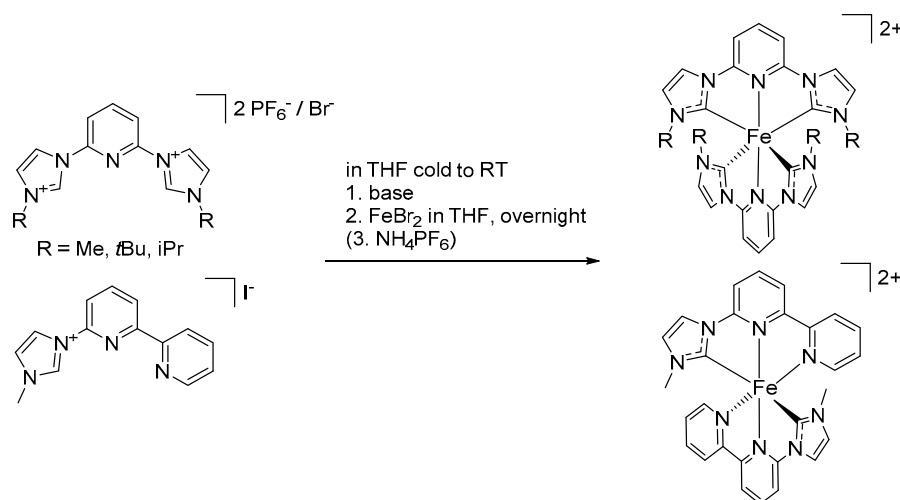


Figure 17. Schematic description of the synthetic procedure using tetrahydrofuran (THF) as a solvent [21,24,32].

A very swift synthetic approach was first reported for $[\text{Fe}(\text{pbhi})_2]^{2+}$, featuring *n*-hexyl groups as *N*-substituents of the imidazolylidene units (Figure 18). Here, the ligand was dissolved in acetonitrile at RT and subsequently treated with FeCl_2 and $\text{KO}t\text{Bu}$ as the base. After just 10 min reaction time, the crude product was precipitated by addition of an aqueous solution of KPF_6 . Silica column chromatography was chosen for the purification which required the use of a 10:3:1 mixture of acetone/water/ KNO_3 (sat) as an eluent. Subsequently the product was reprecipitated by addition of KPF_6 and removal of acetone, leading to a 20% yield [22]. Later this strategy was slightly modified by dissolving the ligand and FeCl_2 in DMF at the same time, followed by addition of the base. For $[\text{Fe}(\text{pbmbi})_2]^{2+}$ a similar workup procedure as just mentioned with some adjustments to the acetone/water/ KNO_3 eluent mixture led to 20% yield (Figure 18). For the synthesis of $[\text{Fe}(\text{cpmbi})_2]^{2+}$, an excess of base has to be used due to the presence of the more easily deprotonated carboxylic acid group. This also makes

acidification necessary before precipitating the crude with KPF_6 which results in an overall lower yield of 10% [33]. Another modification of the DMF method involved the use of $\text{KN}(\text{SiMe}_3)_2$ as a base with the concomitant addition of a base and a FeBr_2 solution to the ligand solution giving $[\text{Fe}(\text{pzbmi})_2]^{2+}$, $[\text{Fe}(\text{pzbhi})_2]^{2+}$ and $[\text{Fe}(\text{pmbmi})_2]^{2+}$ in 15%–30% yields.

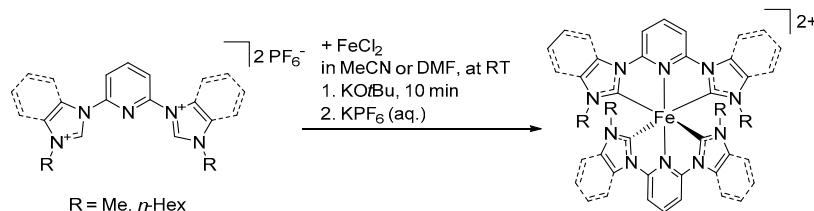


Figure 18. Schematic description of the synthetic procedure using MeCN or *N,N*-dimethylformamide (DMF) as a solvent [22,33].

The synthesis of $[\text{Fe}(\text{cpbmi})_2]^{2+}$ has been reported independently using different procedures for the synthesis of the metal complex [22,23]. The first procedure used DMF and purification by precipitation and washing of the filter residue, leading to a 56% yield of $[\text{Fe}(\text{cpbmi})_2](\text{PF}_6)_2$ [22]. The other reaction was carried out in THF with a purification procedure including multiple filtration steps, treatment with 18-crown-6, to remove excess KPF_6 , and subsection to size-exclusion columns, followed by reprecipitation of the salt, which gave a yield of 18% of the elemental analysis pure $[\text{Fe}(\text{cpbmi})_2](\text{PF}_6)_2$ [23]. This indicates that cumbersome purification protocols might be necessary to obtain pure compounds. Unfortunately, only NMR data is often presented as the sole prove of purity which is blind to contamination by inorganic impurities (e.g., excess KPF_6 which is often used in the final reprecipitation). While such an inorganic impurity would most likely not significantly influence the excited state dynamics (which is the core subject of most of the presented studies) it would still lead to overestimation of the yield and underestimation of the attenuation coefficients. As the field is moving more towards application of photoactive FeNHC complexes, e.g., in DSSC devices or artificial photosynthesis reactions, the presence of impurities and possible influences on the system under investigation should at least be considered.

6.2. Synthesis of Heteroleptic Complexes

The simplest strategy to synthesize heteroleptic complexes is by using an equimolar mixture of two different tridentate ligands and coordinate them to the iron center. This approach was used for the generation of $[\text{Fe}(\text{cpbmi})(\text{pbmi})]^{2+}$, $[\text{Fe}(\text{cpbai})(\text{pbmi})]^{2+}$ and $[\text{Fe}(\text{cpbdpai})(\text{pbmi})]^{2+}$ (Figure 19) from a solution of the corresponding ligands and FeCl_2 in DMF and subsequent addition of KO^tBu [23]. After precipitation under acidic conditions and silica column chromatography, the complexes were obtained in decent 15%–20% yields considering the statistical maximum of 50%.

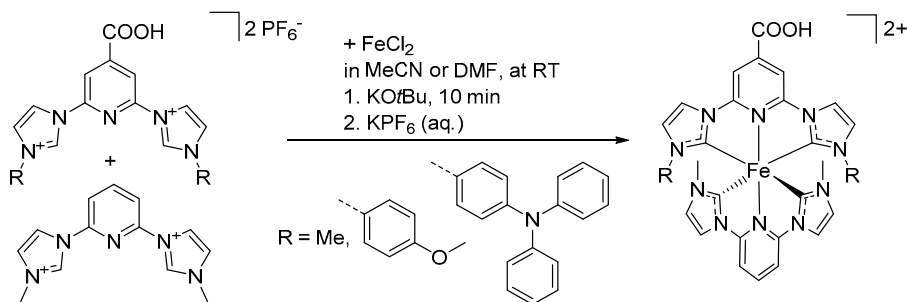


Figure 19. A simple, yet forceful, synthetic approach to heteroleptic FeNHC complexes using 1:1 mixtures of the different ligands [42].

A more targeted path to heteroleptic iron complexes containing NHC ligands is by generating a stable intermediate species, where the iron center is first only coordinated to one tridentate ligand and some auxiliary ligands. One example of this is the synthesis of $[\text{Fe}(\text{pbhi})(\text{pytpy})]^{2+}$ where the pytpy ligand is introduced to FeCl_3 in the first step leading to $[\text{Fe}(\text{pytpy})\text{Cl}_3]$ as an isolated intermediate (Figure 20) [20]. However, this compound is an Fe(III) species that needs to be reduced in situ during the synthesis of $[\text{Fe}(\text{pbhi})(\text{pytpy})]^{2+}$ which leads to a rather low yield of 10% [20]. An improvement to this strategy was achieved by using the pentacoordinate intermediate $[\text{Fe}(\text{pbdppi})\text{Br}_2]$ where a carbene containing ligand is introduced at first (Figure 20). The compound was synthesized from the iron precursor $[\text{Fe}(\text{N}(\text{SiMe}_3)_2)_2(\text{THF})]$ containing two equivalents of inherent base. Thus, the precursor can directly deprotonate and coordinate one pbdppi ligand without extra addition of base. The bulky N-substituents on the imidazolylidene units in pbdppi additionally hinder the coordination of a second ligand leading to $[\text{Fe}(\text{pbdppi})\text{Br}_2]$ [24]. This intermediate has the advantage that it can either be reacted with tpy-type ligands as in the case of $[\text{Fe}(\text{pbdppi})(\text{pytpy})]^{2+}$ and its derivatives or with another carbene-containing ligand which led to $[\text{Fe}(\text{bpymi})(\text{pbdppi})]^{2+}$ (Figure 20). The employed Fe(II) oxidation state in this intermediate also leads to a significant increase in yields of the heteroleptic complexes ranging from 52% to 60% [24,36].

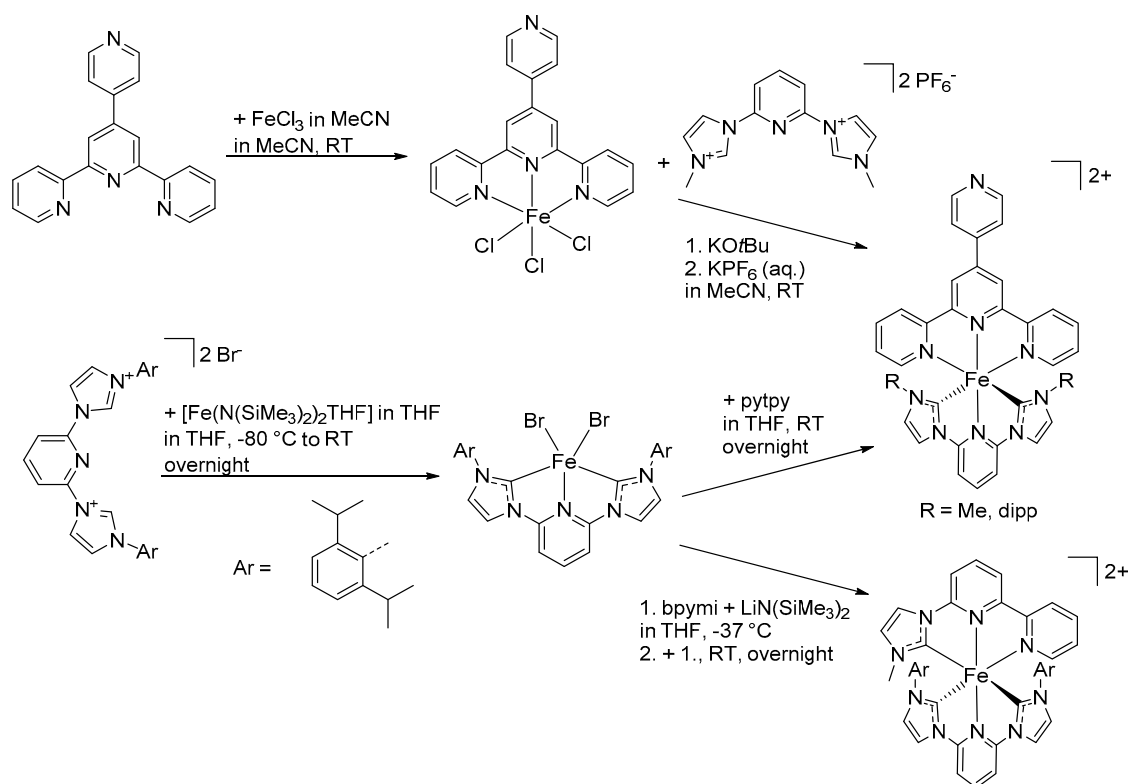


Figure 20. Different synthetic strategies to synthesize pytpy containing FeNHC complexes and heteroleptic FeNHC complexes with two carbene containing ligands [20,24,32].

The pytpy ligand offers the possibility of being modified when coordinated to the iron center thus allowing to influence the properties of the complex by simple means. For instance, protonation and methylation can be achieved leading to a more electron-accepting ligand with the effects described above (c.f., Section 3.2) [20,32]. Even coordination of a chlorobis(dimethylglyoximato)-cobalt(III) motif to the free pyridine unit of the pytpy ligand was achieved but unfortunately this did not lead to the anticipated electron transfer to the Co-moiety in the excited state [32]. Nevertheless, this shows that by suitable choice of ligands and their intelligent modification, the characteristics of the ground state and the excited state dynamics can be influenced and thus give valuable insights in the structure-property-correlation of these compounds.

FeNHC complexes with bidentate ligands have so far been less explored, yet the first example of a photoactive FeNHC complex employing this kind of ligands was the heteroleptic complex $[\text{Fe}(\text{bpy})(\text{btz})_2]^{2+}$ [48]. This compound was synthesized via the high spin intermediate $[\text{Fe}(\text{bpy})\text{Cl}_2]$ which precipitates from the reaction mixture and thus does not react further to the thermodynamically more favored $[\text{Fe}(\text{bpy})_3]^{2+}$ (also facilitated by the excess of iron compared to the bpy ligand employed). The moisture-sensitive intermediate was then reacted with two equivalents of the btz ligand to give $[\text{Fe}(\text{bpy})(\text{btz})_2]^{2+}$ (Figure 21) [48]. This strategy holds the possibility to firstly modify the bpy ligand, although adoption of the solvent system is likely to be necessary, in order to precipitate the tetra-coordinated intermediate, as larger substituents on the bpy are likely to concomitantly change the solubility of the intermediate species. Further, other bidentate ligands could be introduced in the second step (although more promising candidates than the btz ligand are probably hard to find) and even tris-heteroleptic complexes are imaginable if ligand mixtures and/or utilization of steric factors on different ligands are employed.

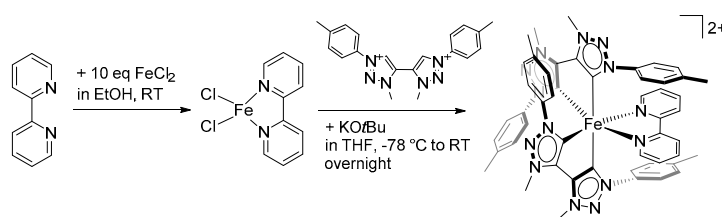


Figure 21. Synthesis of heteroleptic $[\text{Fe}(\text{bpy})(\text{btz})_2]^{2+}$ with bidentate ligands [48].

The use of the non-symmetric mpi ligand led to formation of *fac*- and *mer*-isomers of the final complex $[\text{Fe}(\text{mpi})_3]^{2+}$ that could not be separated (Figure 15) [54]. As the *mer*-isomer is strongly favored (14:1 ratio), a method to force the confirmation to *fac*-coordination was sought. This was achieved by using a hexadentate ligand connecting three pyridine-imidazole units in a tripodal fashion that, upon coordination to iron, leads to $[\text{Fe}(\text{piea})]^{2+}$ which resembles the *fac*-isomer of $[\text{Fe}(\text{mpi})_3]^{2+}$ (Figure 15) [57].

Clearly, the use of NHC-containing ligands imposes stronger synthetic challenges than for instance polypyridine ligands. However, the development of NHC chemistry and its widespread use have led to a broad range of synthetic tools to choose and draw inspiration from. To develop efficient procedures to gain compounds of high purity can be a time- and labor-intense endeavor, but in order to be able to draw meaningful structure-property-correlations, purity is of great importance and it is thus desirable that attention is drawn to this issue.

7. Conclusions and Outlook

Despite the longstanding interest in the photochemistry and photophysics of iron coordination compounds, their application has so far been hampered by their non-ideal photoproperties. Building on knowledge gained from decades of fundamental research and thanks to the properties of NHCs incorporated into the ligand framework, significant progress has been made over the past seven years. The lifetimes of charge separated excited states have been pushed from a few hundred femtoseconds in classical iron polypyridyl complexes to the nanosecond range in the latest generation of FeNHC complexes. Surprisingly, these long-lived and emissive excited states are found in the Fe(III) compounds $[\text{Fe}(\text{btz})_3]^{3+}$ and $[\text{Fe}(\text{phtmb})_2]^+$ with d^5 electron configuration and LMCT excited states in spite of the anticipated MLCT from a d^6 Fe(II) center. The photochemistry of metal complexes with d^5 configuration has so far been rarely explored and mostly involved somewhat exotic Tc(II) and Re(II) metal centers [62]. The recent findings on the Fe(III)NHC complexes might spark more interest for further investigations in d^5 photochemistry and widen the scope beyond the classical photoactive d^6 complexes. Furthermore, it has been shown that $[\text{Fe}(\text{phtmb})_2]^+$ undergoes reductive as well as oxidative quenching from its excited state, which was estimated to have a higher reducing/oxidizing power than $[\text{Ru}(\text{bpy})_3]^{2+}$ [60].

These properties make $[\text{Fe}(\text{phtmib})_2]^+$ an interesting candidate to be employed in photoredox catalysis or artificial photosynthetic approaches based on abundant metal photosensitizers and catalysts. Generally, since the discovery of the beneficial photophysical properties of FeNHC complexes, a shift towards more application-oriented research can be seen without the focus on the fundamental research basis being lost [44]. Hence, a working photocatalytic system for the reduction of protons to hydrogen gas has been presented, albeit with very low turnover numbers [24]. In addition, functioning DSSCs employing FeNHC PSs have been reported and continuously been modified. The overall efficiencies have been lifted from 0.1% to almost 1%; interestingly though, this was achieved mostly by optimizing other cell parameters while using the same dye-molecule, $[\text{Fe}(\text{cpbmi})_2](\text{PF}_6)_2$ [22,43,45]. Therefore, new generations of FeNHC sensitizers have a good chance to achieve more competitive performances. At the same time, most of the herein presented systems have been investigated by a range of spectroscopic methods, ranging from optical and (spectro)electrochemical investigations over spin-sensitive methods to time-resolved optical and various X-ray techniques, often complemented or guided by quantum chemical studies. This clearly shows that research on photoactive FeNHC complexes benefits from a collaborative, interdisciplinary research environment and underlines the importance of an exchange of ideas among different groups of researchers as well as the continuous need for fundamental research to lead the progress.

So far, the extension of the CT excited state lifetimes has arguably been the focus of research on photoactive FeNHC coordination compounds and thus has also seen the greatest development. However, it is not only the lifetime of the photoactive excited state that matters and other properties need to be taken into account as well: ground- and excited state redox potentials need to be of suitable kind to drive the desired process after photoexcitation and allow recovery of the original oxidation state by redox mediators or sacrificial agents. For solar-energy conversion purposes, a broad absorption range and high attenuation coefficients are desirable. Yet, some of these properties are rather influenced collaterally than being rationally designed. While the CT excited state lifetime has been significantly increased, some of the presented compounds have comparably low extinction coefficients ($<5000 \text{ M}^{-1} \text{ cm}^{-1}$) and/or narrow absorption windows, which is not ideal for energy conversion applications. Furthermore, strongly shifted potentials for the Fe(III/II) couple have been observed, which could for instance impede their use with certain redox mediators in DSSCs or lead to oxidation of the complex to Fe(III) under ambient conditions which in turn fundamentally changes the photophysical properties of these compounds, in a favorable or non-favorable direction, depending on application. Therefore, the design of new generations of ligands needs not only to address destabilization of the e_g^* orbitals that correlate to the MC states but also stabilization of t_{2g} orbitals to keep the ground state redox potential in a reasonable range. At the same time the ligand π^* orbitals need to be of suitable energy to accommodate the electron in a MLCT excited state. Creative solutions to this multi-dimensional problem are sought and the future will show what ideas chemists will produce (and be able to synthetically realize) to tackle the mentioned problems. The use of NHC containing ligands has led to significant progress in this research field, however, other approaches have also made big steps forward recently. Cyclometallating ligands have been proposed to have very beneficial properties due to their strong σ -donating character [63–67]. Recently, the first synthesis of an air-stable cyclometallated iron complex has been presented along with investigations of the excited state properties of the compound and a 0.8 ps MLCT lifetime was found (a 5.5-fold increase compared to the 140 fs in the parent $[\text{Fe}(\text{tpy})_2]^{2+}$) [68]. Furthermore, the use of ligands with an amido motif that lead to strong mixing of filled ligand and metal orbitals, combined with a phenanthridine moiety that has low-lying π^* orbitals, produced Fe(II) complexes with MLCT-type excited state lifetimes exceeding 2 ns and broad absorption in the visible spectrum [68]. Considering the progress made and the challenges lying ahead, the photochemistry of iron-based coordination compounds remains an interesting and vibrant field of research.

Author Contributions: Conceptualization, S.K. and K.W.; writing—original draft preparation, S.K.; writing—review and editing, K.W. All authors have read and agreed to the published version of the manuscript.

Funding: S.K. gratefully acknowledges a scholarship from Wenner-Gren Stiftelserna (The Wenner-Gren Foundations). K.W. thanks the Swedish Research Council, the LMK foundation, the Swedish Foundation for Strategic Research, and the Knut and Alice Wallenbergs Stiftelse for generous grants.

Acknowledgments: Yizhu Liu is gratefully acknowledged for helpful comments.

Conflicts of Interest: The authors declare no conflict of interest.

Abbreviations

bpy	2,2'-bipyridine
bpymi	([2,2'-bipyridin]-6-yl)-3-methyl-imidazol-2-ylidene)
btz	4,4'-bis(1,2,3-triazol-5-ylidene)
CoCl(dmgl) ₂	chloro-bis(dimethylglyoximate)-cobalt(III)
cpbdpai	(carboxypyridine-2,6-diyl)bis(1- <i>N,N</i> -diphenylaniliny)-imidazol-2-ylidene)
cpbai	(carboxypyridine-2,6-diyl)bis(1- <i>p</i> -anisyl-imidazol-2-ylidene)
cpbmbi	(carboxypyridine-2,6-diyl)bis(1-methyl-benzimidazol-2-ylidene)
cpbmi	(carboxypyridine-2,6-diyl)bis(1-methyl-imidazol-2-ylidene)
CT	charge transfer
CV	cyclic voltammetry
dcpp	2,6-bis(2-carboxypyridyl)pyridine
ddpd	<i>N,N'</i> -dimethyl- <i>N,N'</i> -dipyridine-2-yl-pyridine-2,6-diamine
DFT	density functional theory
DMF	<i>N,N</i> -dimethylformamide
DSSC	dye-sensitized solar cell
EDG	electron-donating group
EPR	electron paramagnetic resonance
EWG	electron-withdrawing group
Fc	ferrocene
Fe–Co	[Fe(pbdppi)(pytpy)CoCl(dmgl)] ²⁺
FeNHC	iron <i>N</i> -heterocyclic carbene (complex)
GS	ground state
HOMO	highest occupied molecular orbital
IC	internal conversion
ISC	intersystem crossing
I _{SC}	short circuit current
LC	ligand centered
LIESST	light-induced excited state spin trapping
LMCT	ligand-to-metal charge transfer
LUMO	lowest unoccupied molecular orbital
MC	metal centered
MLCT	metal-to-ligand charge transfer
MO	molecular orbital
mpi	3-methyl-1-(pyridin-2-yl)-imidazol-2-ylidene
NHC	<i>N</i> -heterocyclic carbene
NP	nanoparticle
NTO	natural transition orbital
oNTO	occupied natural transition orbital
pbbi	(pyridine-2,6-diyl)bis(1- <i>tert</i> -butyl)-imidazol-2-ylidene)
pbdppi	(pyridine-2,6-diyl)bis(1-(2,6-diisopropylphenyl)-imidazol-2-ylidene)
pbbi	(pyridine-2,6-diyl)bis(1-hexyl-imidazol-2-ylidene)
pmbi	(pyridine-2,6-diyl)bis(1-methyl-benzimidazol-2-ylidene)
pbbi	(pyridine-2,6-diyl)bis(1-methyl-imidazol-2-ylidene)
pbbi	(pyridine-2,6-diyl)bis(1-isopropyl-imidazol-2-ylidene)

pbRi	(pyridine-2,6-diyl)bis(1-alkyl/aryl-imidazol-2-ylidene)
PES	potential energy surface
phtmb	phenyl(tris(3-methylimidazol-2-ylidene))borate
pmbmi	(pyrimidine-2,4-diyl)bis(1-methyl-imidazol-2-ylidene)
PS	photosensitizer
pytpy	(4'-(pyridin-4-yl)-2,2':6',2''-terpyridine)
pytpyH	6'-(pyridin-2-yl)-[2,2':4',4''-terpyridin]-1''-ium
pytpyMe	1''-methyl-6'-(pyridin-2-yl)-[2,2':4',4''-terpyridin]-1''-ium
pzbhbi	(pyrazine-2,6-diyl)bis(1-hexyl-benzimidazol-2-ylidene)
pzbhi	(pyrazine-2,6-diyl)bis(1-hexyl-imidazol-2-ylidene)
pzbmi	(pyrazine-2,6-diyl)bis(1-methyl-imidazol-2-ylidene)
QC	quantum chemical/chemistry
RT	room temperature
SCE	saturated calomel electrode
SEC	spectroelectrochemistry
TCSPC	time-correlated single photon counting
TD-DFT	time-dependent density functional theory
THF	tetrahydrofuran
tpiea	tris(2-(1-(pyridin-2-yl)-imidazol-2-ylidene)ethyl)amine
tpy	2,2':6',2''-terpyridine
TRIS	hydro(tris(3-methylimidazol-2-ylidene))borate
TRWAXS	time-resolved wide-angle X-ray scattering
vNTO	virtual natural transition orbital

Appendix A

Table A1. Overview of absorption maxima, attenuation coefficients and lifetimes of CT states as well as Fe(III/II) redox couple and number of NHC donors of the presented FeNHC complexes.

Acronym	λ_{CT} [nm]	ϵ_{CT} [M ⁻¹ cm ⁻¹]	τ_{CT} [ps]	Fe(III/II) vs. Fc ⁺ /Fc [V]	Fe(III/II) vs. SCE [V]	n NHC donors	Refs.
[Fe(tpy) ₂] ²⁺	495 552	7500 14800	0.1	0.70	1.09 ¹	0	[22]
[Fe(pbmi) ₂] ²⁺	390 457	9100 15200	9	0.31	0.60 ¹	4	[22]
[Fe(pbbi) ₂] ²⁺	412 478	8400 14800	0.3	0.40	0.79 ¹	4	[22]
[Fe(pbhi) ₂] ²⁺	393 460	9000 15900	n/a	0.41	0.80 ¹	4	[21]
[Fe(pbpri) ₂] ²⁺	392 458	9000 15000	8	0.43	0.82 ¹	4	[25,33]
[Fe(bpymi) ₂] ²⁺	419 508 557	4100 4700 7000	<0.1	0.44	0.83 ¹	2	[33]
[Fe(pbmbi) ₂] ²⁺	360 440	9000 12500	16	0.65 ²	1.04	4	[34]
[Fe(pzbmi) ₂] ²⁺	389 487	6300 16100	21–25	0.59 ²	0.98	4	[36]
[Fe(pzbhi) ₂] ²⁺	392 493	6200 17300	22	0.70 ²	1.09	4	[36]
[Fe(pzbhbi) ₂] ²⁺	350 479	11000 16200	32	0.83 ²	1.22	4	[36]
[Fe(pmbmi) ₂] ²⁺	406 477	8500 12600	11–12	0.54 ²	0.93	4	[36]
[Fe(pbhi)(pytpty)] ²⁺	373 522 560	9000 9500 9000	n/a	0.54	0.93 ¹	2	[21]
[Fe(pbhi)(pytptyH)] ³⁺	407 525 590	6400 9000 11500	n/a	0.56	0.95 ¹	2	[21]
[Fe(pbdppi)(tpy)] ²⁺	378 502 540	9000 10000 9500	<0.1	0.56	0.95 ¹	2	[25]
[Fe(bpymi)(pdpipi)] ²⁺	376 409 466 506 538	5500 6400 5200 5000 5300	3.6	0.46	0.85 ¹	3	[33]
[Fe(pbdppi)(pytpty)] ²⁺	375 515 553	9600 10000 9800	1.1	0.60	0.99 ¹	2	[37]
[Fe(pbdppi)(pytptyMe)] ³⁺	374 411 538 586	6600 7000 9900 12700	n/a	0.66	1.05 ¹	2	[37]
Fe–Co	370 520 558	10300 9300 9400	1.4	0.63	1.02 ¹	2	[37]
[Fe(cpbmi) ₂] ²⁺	394 520	7000 16200	17	0.46 ²	0.85	4	[23,24,34]
[Fe(cpbmbi) ₂] ²⁺	370 501	5000 12800	26	0.74 ²	1.13	4	[34]
[Fe(cpbmi)(pbmi)] ²⁺	394 433 506	7625 7050 12650	14	0.43 ²	0.82	4	[43]
[Fe(cpbai)(pbmi)] ²⁺	396 428 509	10100 8540 17700	10	0.42 ²	0.81	4	[43]
[Fe(cpbpai)(pbmi)] ²⁺	395 431 509	6115 5075 9500	12	0.41 ²	0.82	4	[43]
[Fe(bpy) ₃] ²⁺	349 486 520	6030 6880 7980	0.1	0.68	1.07 ¹	0	[49]
[Fe(bpy)(btz) ₂] ²⁺	432 609	5080 3260	13	−0.35	0.04 ¹	4	[49]
[Fe(btz) ₃] ²⁺	370 446 510 688	4600 5500 4000 2000	528	−0.58	−0.19 ¹	6	[50,51]
[Fe(btz) ₃] ³⁺	384 420 528 558	2400 1800 15001400	100	−0.58	−0.19 ¹	6	[51]
[Fe(phtmbi) ₂] ⁺	502	3000	1960	−1.16	−0.77 ¹	6	[61]
[Fe(mpi) ₃] ²⁺	360 430	4500 12000	15–20 ³	0.26 ²	0.65	3	[55,56]
[Fetpiea] ²⁺	369 438	5200 8000	15–20 ³	0.22 ²	0.61	3	[55,56]

¹ Calculated by adding 0.39 V to the value vs. Fc⁺/Fc, ² calculated by subtracting 0.39 V from the value vs. SCE, ³ clear assignment to a CT state is not possible in this case.

References

1. Stephenson, C.R.J.; Yoon, T.P.; MacMillan, D.W.C. (Eds.) *Visible Light Photocatalysis in Organic Chemistry*; Wiley-VCH Verlag GmbH & Co. KGaA: Weinheim, Germany, 2018.
2. Yuan, Y.-J.; Yu, Z.-T.; Chen, D.-Q.; Zou, Z.-G. Metal-complex chromophores for solar hydrogen generation. *Chem. Soc. Rev.* **2017**, *46*, 603–631. [[CrossRef](#)]
3. Yamamoto, M.; Tanaka, K. Artificial molecular photosynthetic systems: Towards efficient photoelectrochemical water oxidation. *ChemPlusChem* **2016**, *81*, 1028–1044. [[CrossRef](#)]
4. Junge, H.; Rockstroh, N.; Fischer, S.; Brückner, A.; Ludwig, R.; Lochbrunner, S.; Kühn, O.; Beller, M. Light to hydrogen: Photocatalytic hydrogen generation from water with molecularly-defined iron complexes. *Inorganics* **2017**, *5*, 14. [[CrossRef](#)]
5. Armaroli, N.; Balzani, V. Solar electricity and solar fuels: Status and perspectives in the context of the energy transition. *Chem. A Eur. J.* **2016**, *22*, 32–57. [[CrossRef](#)] [[PubMed](#)]
6. Balzani, V.; Campagna, S. (Eds.) *Photochemistry and Photophysics of Coordination Compounds I*; Springer: Berlin/Heidelberg, Germany, 2007. [[CrossRef](#)]
7. Campagna, S.; Puntoriero, F.; Nastasi, F.; Bergamini, G.; Balzani, V. *Photochemistry and Photophysics of Coordination Compounds II*; Springer: Berlin/Heidelberg, Germany, 2007. [[CrossRef](#)]
8. Wenger, O.S. Photoactive complexes with earth-abundant metals. *J. Am. Chem. Soc.* **2018**, *140*, 13522–13533. [[CrossRef](#)]
9. Hockin, B.M.; Li, C.; Robertson, N.; Zysman-Colman, E. Photoredox catalysts based on earth-abundant metal complexes. *Catal. Sci. Technol.* **2019**, *9*, 889–915. [[CrossRef](#)]
10. Chen, J.; Browne, W.R. Photochemistry of iron complexes. *Coord. Chem. Rev.* **2018**, *374*, 15–35. [[CrossRef](#)]
11. Wikipedia—Abundance of Elements in Earth's Crust (n.d.). Available online: https://en.wikipedia.org/wiki/Abundance_of_elements_in_Earth%27s_crust (accessed on 11 October 2019).
12. Lindh, L.; Chábera, P.; Rosemann, N.W.; Uhlig, J.; Wärnmark, K.; Yartsev, A.; Sundström, V.; Persson, P. Photophysics and Photochemistry of Iron Carbene Complexes for Solar Energy Conversion and Photocatalysis. *Catalysts*. in press.
13. Wenger, O.S. Is Iron the new ruthenium? *Chem. A Eur. J.* **2019**, *25*, 6043–6052. [[CrossRef](#)]
14. McCusker, J.K. Electronic structure in the transition metal block and its implications for light harvesting. *Science* **2019**, *363*, 484–488. [[CrossRef](#)]
15. Fink, D.W.; Ohnesorge, W.E. Temperature effects on charge-transfer luminescence intensity of some transition metal ion chelates. *J. Am. Chem. Soc.* **1969**, *91*, 4995–4998. [[CrossRef](#)]
16. Decurtins, S.; Gutlich, P.; Hasselbach, K.M.; Hauser, A.; Spiering, H. Light-induced excited-spin-state trapping in iron(II) spin-crossover systems. Optical spectroscopic and magnetic susceptibility study. *Inorg. Chem.* **1985**, *24*, 2174–2178. [[CrossRef](#)]
17. Kahn, O. Spin-transition polymers: From molecular materials toward memory devices. *Science* **1998**, *279*, 44–48. [[CrossRef](#)]
18. Gütlich, P.; Gaspar, A.B.; Garcia, Y. Spin state switching in iron coordination compounds. *Beilstein J. Org. Chem.* **2013**, *9*, 342–391. [[CrossRef](#)] [[PubMed](#)]
19. Jamula, L.L.; Brown, A.M.; Guo, D.; McCusker, J.K. Synthesis and characterization of a high-symmetry ferrous polypyridyl complex: Approaching the 5 T_{2/3} T₁ crossing point for Fe II. *Inorg. Chem.* **2014**, *53*, 15–17. [[CrossRef](#)] [[PubMed](#)]
20. Duchanois, T.; Etienne, T.; Beley, M.; Assfeld, X.; Perpète, E.A.; Monari, A.; Gros, P.C. Heteroleptic pyridyl-carbene Iron complexes with tuneable electronic properties. *Eur. J. Inorg. Chem.* **2014**, *2014*, 3747–3753. [[CrossRef](#)]
21. Liu, Y.; Harlang, T.; Canton, S.E.; Chábera, P.; Suárez-Alcántara, K.; Fleckhaus, A.; Vithanage, D.A.; Göransson, E.; Corani, A.; Lomoth, R.; et al. Towards longer-lived metal-to-ligand charge transfer states of iron(ii) complexes: An N-heterocyclic carbene approach. *Chem. Commun.* **2013**, *49*, 6412. [[CrossRef](#)] [[PubMed](#)]
22. Duchanois, T.; Etienne, T.; Cebrián, C.; Liu, L.; Monari, A.; Beley, M.; Assfeld, X.; Haacke, S.; Gros, P.C. An Iron-based photosensitizer with extended excited-state lifetime: Photophysical and photovoltaic properties. *Eur. J. Inorg. Chem.* **2015**, *2015*, 2469–2477. [[CrossRef](#)]

23. Harlang, T.C.B.; Liu, Y.; Gordivska, O.; Fredin, L.A.; Ponseca, C.S.; Huang, P.; Chábera, P.; Kjaer, K.S.; Mateos, H.; Uhlig, J.; et al. Iron sensitizer converts light to electrons with 92% yield. *Nat. Chem.* **2015**, *7*, 883–889. [[CrossRef](#)]
24. Zimmer, P.; Müller, P.; Burkhardt, L.; Schepper, R.; Neuba, A.; Steube, J.; Dietrich, F.; Flörke, U.; Mangold, S.; Gerhards, M.; et al. *N*-Heterocyclic carbene complexes of Iron as photosensitizers for light-induced water reduction. *Eur. J. Inorg. Chem.* **2017**, *2017*, 1504–1509. [[CrossRef](#)]
25. Clayden, J.; Greeves, N.; Warren, S. *Organic Chemistry*, 2nd ed.; Oxford University Press: Oxford, UK, 2012.
26. Fatur, S.M.; Shepard, S.G.; Higgins, R.F.; Shores, M.P.; Damrauer, N.H. A synthetically tunable system to control MLCT excited-state lifetimes and spin states in Iron(II) polypyridines. *J. Am. Chem. Soc.* **2017**, *139*, 4493–4505. [[CrossRef](#)]
27. Winkler, J.R.; Creutz, C.; Sutin, N. Solvent tuning of the excited-state properties of (2,2'-bipyridine) tetracyanoferrate(II): Direct observation of a metal-to-ligand charge-transfer excited state of Iron(II). *J. Am. Chem. Soc.* **1987**, *109*, 3470–3471. [[CrossRef](#)]
28. Mengel, A.K.C.; Förster, C.; Breivogel, A.; Mack, K.; Ochsmann, J.R.; Laquai, F.; Ksenofontov, V.; Heinze, K. A heteroleptic push-pull substituted Iron(II) bis(tridentate) complex with low-energy charge-transfer states. *Chem. A Eur. J.* **2015**, *21*, 704–714. [[CrossRef](#)] [[PubMed](#)]
29. Liu, Y.; Persson, P.; Sundström, V.; Wärnmark, K. Fe *N*-Heterocyclic carbene complexes as promising photosensitizers. *Acc. Chem. Res.* **2016**, *49*, 1477–1485. [[CrossRef](#)] [[PubMed](#)]
30. Leshchev, D.; Harlang, T.C.B.; Fredin, L.A.; Khakhulin, D.; Liu, Y.; Biasin, E.; Laursen, M.G.; Newby, G.E.; Haldrup, K.; Nielsen, M.M.; et al. Tracking the picosecond deactivation dynamics of a photoexcited iron carbene complex by time-resolved X-ray scattering. *Chem. Sci.* **2018**, *9*, 405–414. [[CrossRef](#)]
31. Fredin, L.A.; Pápai, M.; Rozsályi, E.; Vankó, G.; Wärnmark, K.; Sundström, V.; Persson, P. Exceptional excited-state lifetime of an Iron(II)—*N*-Heterocyclic carbene complex explained. *J. Phys. Chem. Lett.* **2014**, *5*, 2066–2071. [[CrossRef](#)]
32. Zimmer, P.; Burkhardt, L.; Friedrich, A.; Steube, J.; Neuba, A.; Schepper, R.; Müller, P.; Flörke, U.; Huber, M.; Lochbrunner, S.; et al. The connection between NHC ligand count and photophysical properties in Fe(II) photosensitizers: An experimental study. *Inorg. Chem.* **2018**, *57*, 360–373. [[CrossRef](#)]
33. Liu, L.; Duchanois, T.; Etienne, T.; Monari, A.; Beley, M.; Assfeld, X.; Haacke, S.; Gros, P.C. A new record excited state 3MLCT lifetime for metalorganic iron(II) complexes. *Phys. Chem. Chem. Phys.* **2016**, *18*, 12550–12556. [[CrossRef](#)]
34. Gaggioli, C.A.; Bistoni, G.; Ciancaleoni, G.; Tarantelli, F.; Belpassi, L.; Belanzoni, P. Modulating the bonding properties of *N*-Heterocyclic Carbenes (NHCs): A systematic charge-displacement analysis. *Chem. A Eur. J.* **2017**, *23*, 7558–7569. [[CrossRef](#)]
35. Darari, M.; Domenichini, E.; Francés-Monerris, A.; Cebrián, C.; Magra, K.; Beley, M.; Pastore, M.; Monari, A.; Assfeld, X.; Haacke, S.; et al. Iron(II) complexes with diazanyl-NHC ligands: Impact of π -deficiency of the azine core on photophysical properties. *Dalton Trans.* **2019**. [[CrossRef](#)]
36. Zimmer, P.; Burkhardt, L.; Schepper, R.; Gosztola, D.; Zheng, K.; Neuba, A.; Flörke, U.; Wölper, C.; Schoch, R.; Gawelda, W.; et al. Towards noble-metal free dyads: Ground and excited state tuning by a cobalt dimethylglyoxime catalyst connected to an iron *N*-heterocyclic carbene photosensitizer. *Eur. J. Inorg. Chem.* **2018**. [[CrossRef](#)]
37. Francés-Monerris, A.; Gros, P.C.; Pastore, M.; Assfeld, X.; Monari, A. Photophysical properties of bichromophoric Fe(II) complexes bearing an aromatic electron acceptor. *Chem. Acc.* **2019**, *138*, 86. [[CrossRef](#)]
38. Ferrere, S.; Gregg, B.A. Photosensitization of TiO₂ by [Fe^{II}(2,2'-bipyridine-4,4'-dicarboxylic acid)₂(CN)₂]: Band selective electron injection from ultra-short-lived excited states. *J. Am. Chem. Soc.* **1998**, *120*, 843–844. [[CrossRef](#)]
39. Ferrere, S. New photosensitizers based upon [Fe(L)₂(CN)₂] and [Fe(L)₃] (L = Substituted 2,2'-Bipyridine): Yields for the photosensitization of TiO₂ and effects on the band selectivity. *Chem. Mater.* **2000**, *12*, 1083–1089. [[CrossRef](#)]
40. Abrahamsson, M. Solar energy conversion using iron polypyridyl type photosensitizers—A viable route for the future? *Photochemistry* **2017**, *44*, 285–295. [[CrossRef](#)]
41. Fredin, L.A.; Wärnmark, K.; Sundström, V.; Persson, P. Molecular and interfacial calculations of Iron(II) light harvesters. *ChemSusChem* **2016**, *9*, 667–675. [[CrossRef](#)]

42. Pastore, M.; Duchanois, T.; Liu, L.; Monari, A.; Assfeld, X.; Haacke, S.; Gros, P.C. Interfacial charge separation and photovoltaic efficiency in Fe(II)-carbene sensitized solar cells. *Phys. Chem. Chem. Phys.* **2016**, *18*, 28069–28081. [[CrossRef](#)] [[PubMed](#)]
43. Karpacheva, M.; Housecroft, C.E.; Constable, E.C. Electrolyte tuning in dye-sensitized solar cells with N-heterocyclic carbene (NHC) Iron(II) sensitizers. *Beilstein J. Nanotechnol.* **2018**, *9*, 3069–3078. [[CrossRef](#)]
44. Karpacheva, M.; Wyss, V.; Housecroft, C.E.; Constable, E.C. There Is a Future for N-Heterocyclic Carbene Iron(II) Dyes in Dye-Sensitized Solar Cells: Improving Performance through Changes in the Electrolyte. *Materials* **2019**, *12*, 4181. [[CrossRef](#)]
45. Marchini, E.; Darari, M.; Lazzarin, L.; Boaretto, R.; Argazzi, R.; Bignozzi, C.A.; Gros, P.C.; Caramori, S. Recombination and regeneration dynamics in FeNHC(II)-sensitized solar cells. *Chem. Commun.* **2020**, *56*, 2–5. [[CrossRef](#)]
46. Duchanois, T.; Liu, L.; Pastore, M.; Monari, A.; Cebrián, C.; Trolez, Y.; Darari, M.; Magra, K.; Francés-Monerris, A.; Domenichini, E.; et al. NHC-based Iron sensitizers for DSSCs. *Inorganics* **2018**, *6*, 63. [[CrossRef](#)]
47. Liu, Y.; Wärnmark, K. Fe complexes as photosensitizers for dye-sensitized solar cells. In *Emerging Photovoltaic Technologies: Photophysics and Devices*, 1st ed.; Ponseca, C.S., Ed.; Jenny Stanford Publishing: Singapore, 2020.
48. Liu, Y.; Kjaer, K.S.; Fredin, L.A.; Chábera, P.; Harlang, T.; Canton, S.E.; Lidin, S.; Zhang, J.; Lomoth, R.; Bergquist, K.-E.; et al. A heteroleptic ferrous complex with mesoionic bis(1,2,3-triazol-5-ylidene) ligands: Taming the MLCT excited state of Iron(II). *Chem. A Eur. J.* **2015**, *21*, 3628–3639. [[CrossRef](#)] [[PubMed](#)]
49. Chábera, P.; Kjaer, K.S.; Prakash, O.; Honarfar, A.; Liu, Y.; Fredin, L.A.; Harlang, T.C.B.; Lidin, S.; Uhlig, J.; Sundström, V.; et al. Fe II hexa N-Heterocyclic carbene complex with a 528 ps metal-to-ligand charge-transfer excited-state lifetime. *J. Phys. Chem. Lett.* **2018**, *9*, 459–463. [[CrossRef](#)] [[PubMed](#)]
50. Chábera, P.; Liu, Y.; Prakash, O.; Thyraug, E.; Nahhas, A.; Honarfar, A.; Essén, S.; Fredin, L.A.; Harlang, T.C.B.; Kjær, K.S.; et al. A low-spin Fe(III) complex with 100-ps ligand-to-metal charge transfer photoluminescence. *Nature* **2017**, *543*, 695–699. [[CrossRef](#)] [[PubMed](#)]
51. Tatsuno, H.; Kjaer, K.S.; Kunnus, K.; Harlang, T.C.B.; Timm, C.; Guo, M.; Chábera, P.; Fredin, L.A.; Hartsock, R.W.; Reinhard, M.E.; et al. Hot Branching Dynamics in a Light-Harvesting Iron Carbene Complex Revealed by Ultrafast X-Ray Emission Spectroscopy. *Angew. Chemie Int. Ed.* **2020**, *59*, 364–372. [[CrossRef](#)] [[PubMed](#)]
52. Ericson, F.; Honarfar, A.; Prakash, O.; Tatsuno, H.; Fredin, L.A.; Handrup, K.; Chábera, P.; Gordivska, O.; Kjær, K.S.; Liu, Y.; et al. Electronic structure and excited state properties of iron carbene photosensitizers—A combined X-ray absorption and quantum chemical investigation. *Chem. Phys. Lett.* **2017**, *683*, 559–566. [[CrossRef](#)]
53. Chábera, P.; Fredin, L.A.; Kjær, K.S.; Rosemann, N.W.; Lindh, L.; Prakash, O.; Liu, Y.; Wärnmark, K.; Uhlig, J.; Sundström, V.; et al. Band-selective dynamics in charge-transfer excited iron carbene complexes. *Faraday Discuss.* **2019**, *216*, 191–210. [[CrossRef](#)]
54. Francés-Monerris, A.; Magra, K.; Darari, M.; Cebrián, C.; Beley, M.; Domenichini, E.; Haacke, S.; Pastore, M.; Assfeld, X.; Gros, P.C.; et al. Synthesis and computational study of a pyridylcarbene Fe(II) complex: Unexpected effects of fac/mer isomerism in metal-to-ligand triplet potential energy surfaces. *Inorg. Chem.* **2018**, *57*, 10431–10441. [[CrossRef](#)] [[PubMed](#)]
55. Magra, K.; Domenichini, E.; Francés-Monerris, A.; Cebrián, C.; Beley, M.; Darari, M.; Pastore, M.; Monari, A.; Assfeld, X.; Haacke, S.; et al. Impact of the fac/mer Isomerism on the excited-state dynamics of pyridyl-carbene Fe(II) complexes. *Inorg. Chem.* **2019**, *58*, 5069–5081. [[CrossRef](#)]
56. Forshaw, A.P.; Bontchev, R.P.; Smith, J.M. Oxidation of the tris(carbene)borate complex PhB(MeIm)₃Mn^I(CO)₃ to Mn^{IV}[PhB(MeIm)₃]₂(OTf)₂. *Inorg. Chem.* **2007**, *46*, 3792–3794. [[CrossRef](#)]
57. Kernbach, U.; Ramm, M.; Luger, P.; Fehlhammer, W.P. A chelating triscarbene ligand and its hexacarbene Iron complex. *Angew. Chem. Int. Ed. Engl.* **1996**, *35*, 310–312. [[CrossRef](#)]
58. Muñoz, S.B.; Foster, W.K.; Lin, H.J.; Margarit, C.G.; Dickie, D.A.; Smith, J.M. Tris(carbene)borate ligands featuring imidazole-2-ylidene, benzimidazol-2-ylidene, and 1,3,4-triazol-2-ylidene donors. Evaluation of donor properties in four-coordinate {NiNO}10 complexes. *Inorg. Chem.* **2012**, *51*, 12660–12668. [[CrossRef](#)]

59. Forshaw, A.P.; Smith, J.M.; Ozarowski, A.; Krzystek, J.; Smirnov, D.; Zvyagin, S.A.; Harris, T.D.; Karunadasa, H.I.; Zadrozny, J.M.; Schnegg, A.; et al. Low-spin hexacoordinate Mn(III): Synthesis and spectroscopic investigation of homoleptic tris(pyrazolyl)borate and tris(carbene)borate complexes. *Inorg. Chem.* **2013**, *52*, 144–159. [[CrossRef](#)] [[PubMed](#)]
60. Kjær, K.S.; Kaul, N.; Prakash, O.; Chábera, P.; Rosemann, N.W.; Honarfar, A.; Gordivska, O.; Fredin, L.A.; Bergquist, K.; Häggström, L.; et al. Luminescence and reactivity of a charge-transfer excited iron complex with nanosecond lifetime. *Science* **2019**, *363*, 249–253. [[CrossRef](#)] [[PubMed](#)]
61. Zhou, H.; Zhang, W.-Z.; Liu, C.-H.; Qu, J.-P.; Lu, X.-B. CO₂ adducts of *N*-Heterocyclic carbenes: Thermal stability and catalytic activity toward the coupling of CO₂ with epoxides. *J. Org. Chem.* **2008**, *73*, 8039–8044. [[CrossRef](#)] [[PubMed](#)]
62. Chábera, P.; Lindh, L.; Rosemann, N.W.; Prakash, O.; Uhlig, J.; Yartsev, A.; Wärnmark, K.; Sundström, V.; Persson, P. Photofunctionality of Iron (III) *N*-Heterocyclic Carbenes and Related d⁵ Transition Metal Complexes. *Coord. Chem. Rev.* **2020**, in press.
63. Dixon, I.M.; Khan, S.; Alary, F.; Boggio-Pasqua, M.; Heully, J.L. Probing the photophysical capability of mono and bis(cyclometallated) Fe(II) polypyridine complexes using inexpensive ground state DFT. *Dalt. Trans.* **2014**, *43*, 15898–15905. [[CrossRef](#)]
64. Dixon, I.M.; Alary, F.; Boggio-Pasqua, M.; Heully, J.L. Reversing the relative 3MLCT-3MC order in Fe(II) complexes using cyclometallating ligands: A computational study aiming at luminescent Fe(II) complexes. *Dalt. Trans.* **2015**, *44*, 13498–13503. [[CrossRef](#)]
65. Mukherjee, S.; Bowman, D.N.; Jakubikova, E. Cyclometalated Fe(II) complexes as sensitizers in dye-sensitized solar cells. *Inorg. Chem.* **2015**, *54*, 560–569. [[CrossRef](#)]
66. Ashley, D.C.; Mukherjee, S.; Jakubikova, E. Designing air-stable cyclometalated Fe(II) complexes: Stabilization via electrostatic effects. *Dalt. Trans.* **2019**, *48*, 374–378. [[CrossRef](#)]
67. Steube, J.; Burkhardt, L.; Pöpcke, A.; Moll, J.; Zimmer, P.; Schoch, R.; Wölper, C.; Heinze, K.; Lochbrunner, S.; Bauer, M. Excited state kinetics of an air-stable cyclometalated iron(II) complex. *Chem. A Eur. J.* **2019**. [[CrossRef](#)] [[PubMed](#)]
68. Braun, J.D.; Lozada, I.B.; Kolodziej, C.; Burda, C.; Newman, K.M.E.; van Lierop, J.; Davis, R.L.; Herbert, D.E. Iron(II) coordination complexes with panchromatic absorption and nanosecond charge-transfer excited state lifetimes. *Nat. Chem.* **2019**, *11*, 1144–1150. [[CrossRef](#)] [[PubMed](#)]



© 2020 by the authors. Licensee MDPI, Basel, Switzerland. This article is an open access article distributed under the terms and conditions of the Creative Commons Attribution (CC BY) license (<http://creativecommons.org/licenses/by/4.0/>).